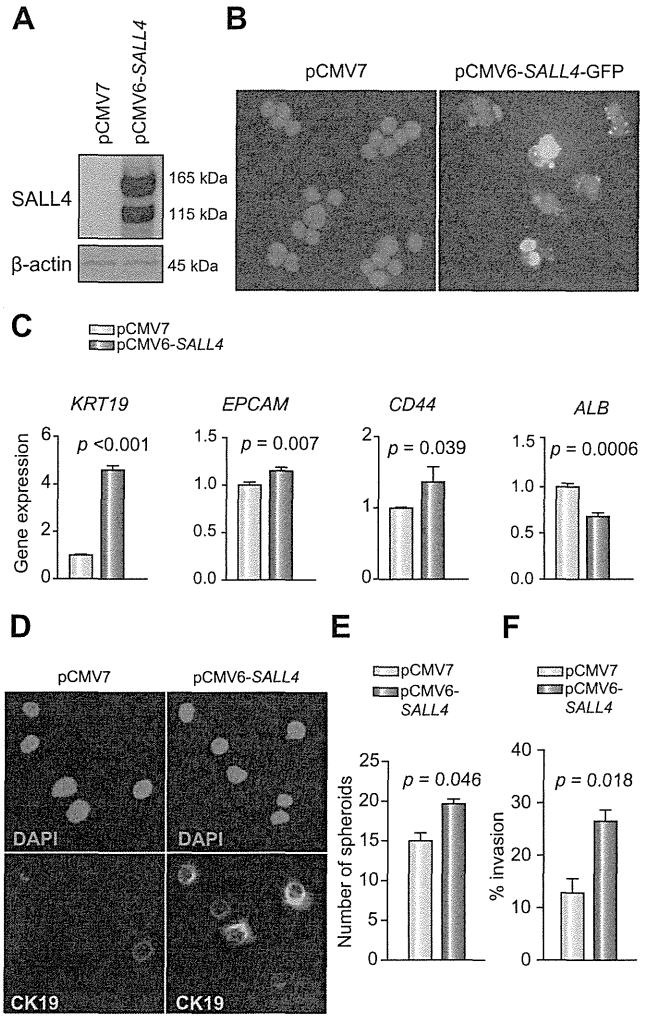

Fig. 3. Effect of SALL4 overexpression. (A) Western blots of cell lysates with anti-SALL4 antibodies. HuH1 cells were transfected with pCMV7 or pCMV6-*SALL4* and incubated for 72 h. (B) IF analysis of HuH1 cells transfected with pCMV7 or pCMV6-*SALL4* and incubated for 72 h. (C) qRT-PCR analysis of *KRT19*, *EPCAM*, *CD44*, and *ALB* in HuH1 cells transfected with pCMV7 or pCMV6-*SALL4* and incubated for 48 h. (D) IF analysis of HuH1 cells transfected with pCMV7 or pCMV6-*SALL4*, incubated for 72 h and stained with anti-CK19 antibodies, evaluated by the confocal laser scanning microscopy. (E) Spheroid formation assay of HuH1 cells transfected with pCMV7 or pCMV6-*SALL4*. Number of spheroids obtained from 2000 cells is indicated (n = 3, mean ± SD). (F) Invasion assay of HuH1 cells transfected with pCMV7 or pCMV6-*SALL4* (n = 3, mean ± SD). (This figure appears in colour on the web.)

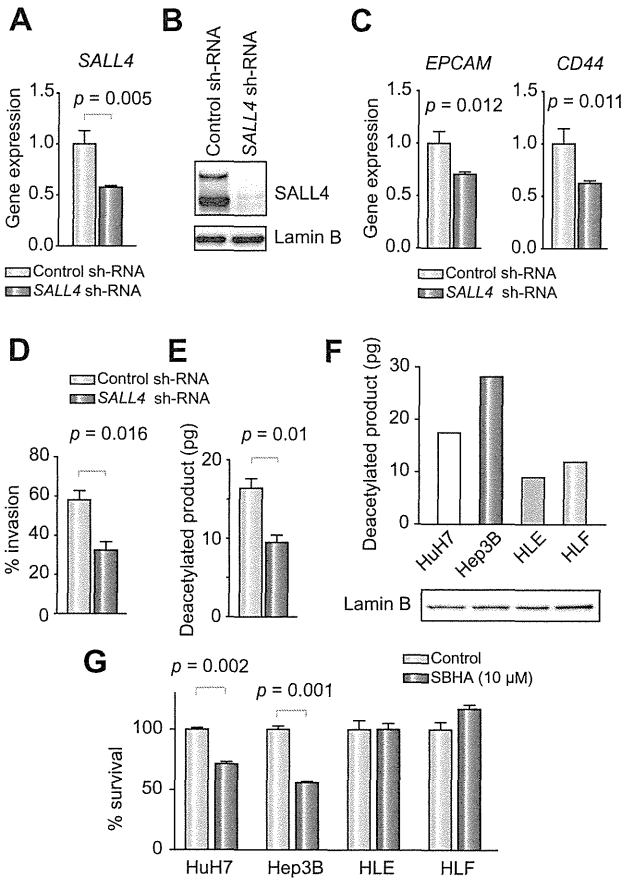

Fig. 4. Effect of *SALL4* knockdown and HDAC activity. (A) qRT-PCR analysis of *SALL4* in HuH7 cells transfected with control or *SALL4* sh-RNAs (n = 3, mean ± SD). (B) Western blots of lysates obtained from HuH7 cells transfected with control or *SALL4* sh-RNAs with anti-SALL4 antibodies. (C) qRT-PCR analysis of *EPCAM* and *CD44* in HuH7 cells transfected with control or *SALL4* sh-RNAs (n = 3, mean ± SD). (D) Invasion assay of HuH7 cells transfected with control or *SALL4* sh-RNAs (n = 3, mean ± SD). (E) HDAC activity of nuclear extracts obtained from HuH7 cells transfected with control or *SALL4* sh-RNAs. (F) HDAC activity of nuclear extracts obtained from each cell line. HDAC activity was measured in duplicate and average amounts of deacetylated products are indicated (upper panel). Lamin B included in the nuclear extracts loaded for HDAC activity assays was measured by Western blotting (lower panel). (G) Cell proliferation assay of HCC cell lines. Each cell line was treated with control DMSO or 10 μM SBHA and cultured for 72 h (n = 4, mean ± SD).

proposed an HCC classification system based on the stem/maturation status of the tumor by EpCAM and AFP expression status [8]. These HCC subtypes showed distinct gene expression patterns with features resembling particular stages of liver lineages. Among them, HpSC-HCC was characterized by a highly invasive nature, chemoresistance to fluorouracil, and poor prognosis after radical resection, warranting the development of a novel therapeutic approach against this HCC subtype [9].

In this study, we showed that the transcription factor SALL4 was activated in HpSC-HCC and that SALL4 might regulate HCC stemness, as characterized by the activation of EpCAM, CK19, and CD44 with highly tumorigenic and invasive natures. Furthermore, we identified that SALL4-positive HCC cell lines tended to show high HDAC activity and chemosensitivity to the HDAC inhibitors SBHA and SAHA. This study reveals for the first time the utility of SBHA for the treatment of HCC with stem cell features.

SALL4 is a zinc finger transcription factor originally cloned based on sequence homology to *Drosophila sal* [11]. *SALL4* mutations are associated with the Okihiro syndrome, a human disease involving multiple organ defects [23,24]. SALL4 plays a fundamental role in the maintenance of embryonic stem cells, potentially through interaction with Oct4, Sox2, and Nanog [25–30]. Furthermore, knockdown of SALL4 significantly reduces the efficiency of induced pluripotent stem cell generation [31]. *SALL4* is also expressed in hematopoietic stem cells and leukemia cells, where it regulates their maintenance [14,32]. SALL4 is known to encode two isoforms (SALL4A and SALL4B), and a recent study

suggested the important role of SALL4B on maintaining the stemness of embryonic stem cells [25]. Interestingly, our data indicated that SALL4B is also a dominant form in HpSC-HCC cell lines. It is unclear how SALL4 isoform expression is regulated in cancer, and future studies are required to explore the mechanisms of SALL4 isoform regulation.

In the liver, SALL4 is expressed in fetal hepatic stem/progenitors but not in adult hepatocytes, and a mouse study demonstrated that inhibition of SALL4 in hepatic stem/progenitors contributes to their differentiation [33]. Interestingly, recent studies indicated that AFP-producing gastric cancer expresses SALL4, suggesting that SALL4 might play a role in the hepatoid differentiation of gastric cancer [34]. Consistently, our data indicated a positive correlation between *SALL4*, *AFP*, and *EPCAM* expression in two independent HCC cohorts. Strikingly, SALL4 was recently shown to be expressed in a subset of human liver cancers with poor prognoses, while modification of SALL4 expression resulted in the alteration of cell proliferation *in vitro* and tumor growth *in vivo*, consistent with our current study [35]. A recent study reported the expression of SALL4 in 46% of HCC cases, which is almost comparable to our present study [36]. Furthermore, a very recent study of two independent large cohorts demonstrated that SALL4 is a marker for a progenitor subclass of HCC with an aggressive phenotype [37]. It is still unclear how SALL4 expression is regulated and which target genes are directly activated by SALL4 binding. Future studies using next generation sequencing are required to fully understand the mechanisms of SALL4 regulation of HCC stemness.

In this study, we demonstrated that SALL4-positive HCC cell lines have high HDAC activity and chemosensitivity against the HDAC inhibitors SBHA and SAHA compared with SALL4-negative HCC cell lines. SALL4 was recently found to directly connect with the epigenetic modulator NuRD complex [22], thereby possibly affecting the histone modification associated with stemness. The NuRD complex is a multiunit chromatin remodeling complex containing chromodomain-helicase-DNA-binding proteins and HDACs that regulate histone deacetylation [38]. Its role in cancer is still controversial, while its function in HCC has not yet been determined.

Our data suggest that SALL4 plays a role in controlling HDAC activity and contributing to the maintenance of HCC with stem cell features. Consistently, HDAC inhibitors might be useful for the eradication of SALL4-positive HCC cells through their inhibitory effects on histone deacetylation by NuRD [39]. Encouragingly, a recent study demonstrated the utility of a SALL4-binding peptide to inhibit its binding to phosphatase and tensin homolog deleted on chromosome 10 (PTEN) through interaction with HDAC, thereby targeting leukemia cells [21]. Further studies are required to understand the relationship between SALL4, the NuRD complex, and the maintenance of stemness in HCC.

Financial support

This study was supported by a Grant-in-Aid from the Ministry of Education, Culture, Sports, Science and Technology, Japan (23590967), a grant from the Japanese Society of Gastroenterology, a grant from the Ministry of Health, Labour and Welfare, and a grant from the National Cancer Center Research and Development Fund (23-B-5), Japan.

Conflict of interest

The authors who have taken part in this study declared that they do not have anything to disclose regarding funding or conflict of interest with respect to this manuscript.

Acknowledgments

We thank Ms. Masayo Baba and Ms. Nami Nishiyama for excellent technical assistance.

Supplementary data

Supplementary data associated with this article can be found, in the online version, at http://dx.doi.org/10.1016/j.jhep.2013.08.024.

References

[1] Nowell PC. The clonal evolution of tumor cell populations. Science 1976;194:23–28.
[2] Hanahan D, Weinberg RA. Hallmarks of cancer: the next generation. Cell 2011;144:646–674.
[3] Jordan CT, Guzman ML, Noble M. Cancer stem cells. N Engl J Med 2006;355:1253–1261.
[4] Clarke MF, Dick JE, Dirks PB, Eaves CJ, Jamieson CH, Jones DL, et al. Cancer stem cells–perspectives on current status and future directions: AACR Workshop on cancer stem cells. Cancer Res 2006;66:9339–9344.
[5] Dean M, Fojo T, Bates S. Tumour stem cells and drug resistance. Nat Rev Cancer 2005;5:275–284.
[6] Visvader JE, Lindeman GJ. Cancer stem cells in solid tumours: accumulating evidence and unresolved questions. Nat Rev Cancer 2008;8:755–768.
[7] Jemal A, Bray F, Center MM, Ferlay J, Ward E, Forman D. Global cancer statistics. CA Cancer J Clin 2011;61:69–90.
[8] Yamashita T, Forgues M, Wang W, Kim JW, Ye Q, Jia H, et al. EpCAM and alpha-fetoprotein expression defines novel prognostic subtypes of hepatocellular carcinoma. Cancer Res 2008;68:1451–1461.
[9] Yamashita T, Ji J, Budhu A, Forgues M, Yang W, Wang HY, et al. EpCAM-positive hepatocellular carcinoma cells are tumor-initiating cells with stem/progenitor cell features. Gastroenterology 2009;136:1012–1024.
[10] Yamashita T, Budhu A, Forgues M, Wang XW. Activation of hepatic stem cell marker EpCAM by Wnt-beta-catenin signaling in hepatocellular carcinoma. Cancer Res 2007;67:10831–10839.
[11] de Celis JF, Barrio R. Regulation and function of spalt proteins during animal development. Int J Dev Biol 2009;53:1385–1398.
[12] Aguila JR, Liao W, Yang J, Avila C, Hagag N, Senzel L, et al. SALL4 is a robust stimulator for the expansion of hematopoietic stem cells. Blood 2011;118:576–585.
[13] Yang J, Chai L, Gao C, Fowles TC, Alipio Z, Dang H, et al. SALL4 is a key regulator of survival and apoptosis in human leukemic cells. Blood 2008;112:805–813.
[14] Yang J, Chai L, Liu F, Fink LM, Lin P, Silberstein LE, et al. Bmi-1 is a target gene for SALL4 in hematopoietic and leukemic cells. Proc Natl Acad Sci U S A 2007;104:10494–10499.
[15] Yamashita T, Honda M, Nio K, Nakamoto Y, Takamura H, Tani T, et al. Oncostatin m renders epithelial cell adhesion molecule-positive liver cancer stem cells sensitive to 5-fluorouracil by inducing hepatocytic differentiation. Cancer Res 2010;70:4687–4697.
[16] Yamashita T, Honda M, Takatori H, Nishino R, Minato H, Takamura H, et al. Activation of lipogenic pathway correlates with cell proliferation and poor prognosis in hepatocellular carcinoma. J Hepatol 2009;50:100–110.
[17] Woo HG, Wang XW, Budhu A, Kim YH, Kwon SM, Tang ZY, et al. Association of TP53 mutations with stem cell-like gene expression and survival of patients with hepatocellular carcinoma. Gastroenterology 2011;140:1063–1070.
[18] Ji J, Wang XW. Clinical implications of cancer stem cell biology in hepatocellular carcinoma. Semin Oncol 2012;39:461–472.

[19] Yang J, Corsello TR, Ma Y. Stem cell gene SALL4 suppresses transcription through recruitment of DNA methyltransferases. J Biol Chem 2012;287: 1996–2005.
[20] Bohm J, Sustmann C, Wilhelm C, Kohlhase J. SALL4 is directly activated by TCF/LEF in the canonical Wnt signaling pathway. Biochem Biophys Res Commun 2006;348:898–907.
[21] Gao C, Dimitrov T, Yong KJ, Tatetsu H, Jeong HW, Luo HR, et al. Targeting transcription factor SALL4 in acute myeloid leukemia by interrupting its interaction with an epigenetic complex. Blood 2013;121:1413–1421.
[22] Lu J, Jeong HW, Kong N, Yang Y, Carroll J, Luo HR, et al. Stem cell factor SALL4 represses the transcriptions of PTEN and SALL1 through an epigenetic repressor complex. PLoS One 2009;4:e5577.
[23] Al-Baradie R, Yamada K, St Hilaire C, Chan WM, Andrews C, McIntosh N, et al. Duane radial ray syndrome (Okihiro syndrome) maps to 20q13 and results from mutations in SALL4, a new member of the SAL family. Am J Hum Genet 2002;71:1195–1199.
[24] Kohlhase J, Heinrich M, Schubert L, Liebers M, Kispert A, Laccone F, et al. Okihiro syndrome is caused by SALL4 mutations. Hum Mol Genet 2002;11:2979–2987.
[25] Rao S, Zhen S, Roumiantsev S, McDonald LT, Yuan GC, Orkin SH. Differential roles of Sall4 isoforms in embryonic stem cell pluripotency. Mol Cell Biol 2010;30:5364–5380.
[26] Tanimura N, Saito M, Ebisuya M, Nishida E, Ishikawa F. Stemness-related factor sall4 interacts with transcription factors oct-3/4 and sox2 and occupies oct-sox elements in mouse embryonic stem cells. J Biol Chem 2013;288:5027–5038.
[27] Wu Q, Chen X, Zhang J, Loh YH, Low TY, Zhang W, et al. Sall4 interacts with nanog and co-occupies nanog genomic sites in embryonic stem cells. J Biol Chem 2006;281:24090–24094.
[28] Yang J, Chai L, Fowles TC, Alipio Z, Xu D, Fink LM, et al. Genome-wide analysis reveals Sall4 to be a major regulator of pluripotency in murine-embryonic stem cells. Proc Natl Acad Sci U S A 2008;105:19756–19761.
[29] Yang J, Gao C, Chai L, Ma Y. A novel SALL4/OCT4 transcriptional feedback network for pluripotency of embryonic stem cells. PLoS One 2010;5:e10766.
[30] Zhang J, Tam WL, Tong GQ, Wu Q, Chan HY, Soh BS, et al. Sall4 modulates embryonic stem cell pluripotency and early embryonic development by the transcriptional regulation of Pou5f1. Nat Cell Biol 2006;8:1114–1123.
[31] Tsubooka N, Ichisaka T, Okita K, Takahashi K, Nakagawa M, Yamanaka S. Roles of Sall4 in the generation of pluripotent stem cells from blastocysts and fibroblasts. Genes Cells 2009;14:683–694.
[32] Yang J, Liao W, Ma Y. Role of SALL4 in hematopoiesis. Curr Opin Hematol 2012;19:287–291.
[33] Oikawa T, Kamiya A, Kakinuma S, Zeniya M, Nishinakamura R, Tajiri H, et al. Sall4 regulates cell fate decision in fetal hepatic stem/progenitor cells. Gastroenterology 2009;136:1000–1011.
[34] Ikeda H, Sato Y, Yoneda N, Harada K, Sasaki M, Kitamura S, et al. Alpha-Fetoprotein-producing gastric carcinoma and combined hepatocellular and cholangiocarcinoma show similar morphology but different histogenesis with respect to SALL4 expression. Hum Pathol 2012;43:1955–1963.
[35] Oikawa T, Kamiya A, Zeniya M, Chikada H, Hyuck AD, Yamazaki Y, et al. SALL4, a stem cell biomarker in liver cancers. Hepatology 2013;57:1469–1483.
[36] Gonzalez-Roibon N, Katz B, Chaux A, Sharma R, Munari E, Faraj SF, et al. Immunohistochemical expression of SALL4 in hepatocellular carcinoma, a potential pitfall in the differential diagnosis of yolk sac tumors. Hum Pathol 2013;44:1293–1299.
[37] Yong KJ, Gao C, Lim JS, Yan B, Yang H, Dimitrov T, et al. Oncofetal gene SALL4 in aggressive hepatocellular carcinoma. N Engl J Med 2013;368: 2266–2276.
[38] Lai AY, Wade PA. Cancer biology and NuRD: a multifaceted chromatin remodelling complex. Nat Rev Cancer 2011;11:588–596.
[39] Marquardt JU, Thorgeirsson SS. Sall4 in "stemness"-driven hepatocarcinogenesis. N Engl J Med 2013;368:2316–2318.

nature medicine

A new cloning and expression system yields and validates TCRs from blood lymphocytes of patients with cancer within 10 days

Eiji Kobayashi[1,4], Eishiro Mizukoshi[2,4], Hiroyuki Kishi[1], Tatsuhiko Ozawa[1], Hiroshi Hamana[1], Terumi Nagai[1], Hidetoshi Nakagawa[2], Aishun Jin[1,3], Shuichi Kaneko[2] & Atsushi Muraguchi[1]

Antigen-specific T cell therapy, or T cell receptor (TCR) gene therapy, is a promising immunotherapy for infectious diseases and cancers. However, a suitable rapid and direct screening system for antigen-specific TCRs is not available. Here, we report an efficient cloning and functional evaluation system to determine the antigen specificity of TCR cDNAs derived from single antigen-specific human T cells within 10 d. Using this system, we cloned and analyzed 380 Epstein-Barr virus–specific TCRs from ten healthy donors with latent Epstein-Barr virus infection and assessed the activity of cytotoxic T lymphocytes (CTLs) carrying these TCRs against antigenic peptide–bearing target cells. We also used this system to clone tumor antigen–specific TCRs from peptide-vaccinated patients with cancer. We obtained 210 tumor-associated antigen–specific TCRs and demonstrated the cytotoxic activity of CTLs carrying these TCRs against peptide-bearing cells. This system may provide a fast and powerful approach for TCR gene therapy for infectious diseases and cancers.

New immunotherapies such as adoptive cell transfer, TCR gene therapy and peptide vaccination have the potential to cure human disease in the future. Rosenberg and his colleagues have reported the adoptive transfer of TCR gene–modified T cells into patients using autologous T cells expressing a TCR recognizing the melanoma-melanocyte differentiation antigen[1,2]. Subsequent clinical trials have targeted antigens such as oncofetal antigen, cancer testis antigen, tissue-specific antigen and overexpressed tumor-associated antigens (TAAs)[3,4]. However, despite its great potential, TCR gene therapy for cancer is still limited to certain tumor antigens and common human leukocyte antigen (HLA) complexes. The conventional approaches for TCR gene cloning involve the establishment of antigen-specific T cell clones, which usually requires several months. Thus, a rapid screening system for antigen-specific TCR genes is needed.

Our group and others have reported single-cell RT-PCR protocols that permit the simultaneous identification of complementarity determining region 3α (CDR3α) and CDR3β transcripts in human[5] and mouse[6] TCRs. However, these protocols cannot retrieve TCRαβ pairs and determine their properties, including antigen specificity and cytotoxicity-inducing activity. In this study, we attempted to establish a direct TCR cloning system that would allow the unbiased analysis of the TCR repertoire, as well as the retrieval of antigen-specific TCRαβ pairs and the characterization of their function for future TCR gene therapy.

RESULTS

Rapid cloning and evaluation of antigen-specific TCRs

We depict the schematic for our rapid cloning and functional assay system, which can obtain TCRαβ cDNA pairs from a single antigen-specific human T cell and confirm their antigen specificity within 10 d (**Fig. 1** and **Supplementary Fig. 1**). This system was designated 'hTEC10' (human TCR efficient cloning within 10 d).

To evaluate the hTEC10 system for analyzing T cells in human disease, we first analyzed Epstein-Barr virus (EBV)-specific $CD8^+$ T cells derived from healthy HLA-$A24^+$ donors with latent EBV infection. We used an HLA-A*2402–restricted major histocompatibility complex (MHC) tetramer mixture of five EBV epitopes (BRLF-1, BMLF-1, latent membrane protein 2 (LMP2), Epstein-Barr nuclear antigen 3A (EBNA3A) and EBNA3B)[7] to detect EBV-specific $CD8^+$ T cells. We detected varying frequencies (0.00–0.64%) of tetramer-positive cells within the $CD8^+$ T cell populations from 19 HLA-$A24^+$ donors (**Fig. 2a** and **Supplementary Table 1**). We then used FACS to sort single tetramer-positive cells from ten donors whose frequencies of tetramer-positive cells were more than 0.06% of $CD8^+$ T cells (with donor I having the minimum frequency of 0.06%). The efficacy of amplifying the TCRα and TCRβ cDNA pairs from the sorted single T cells was 13–72%, using the 5′ rapid amplification of cDNA ends (RACE) method[5] (**Supplementary Table 2**).

We then analyzed the obtained TCR pairs from each donor. A small population expressed dual TCRα, dual TCRβ or both. In some donors, a large number of T cells expressed dual TCRα or dual TCRβ. This may be due to clonal expansion (**Supplementary Table 3**). In total, we obtained 380 EBV-specific TCRs from ten healthy donors with latent EBV infection (**Supplementary Table 2**).

The diversity of the EBV-specific TCRs was highly restricted (from one to ten in each donor) (**Fig. 2b** and **Supplementary Fig. 2**). Because

[1]Department of Immunology, Graduate School of Medicine and Pharmaceutical Sciences, University of Toyama, Toyama, Japan. [2]Department of Gastroenterology, Graduate School of Medicine, Kanazawa University, Kanazawa, Ishikawa, Japan. [3]College of Basic Medical Science, Harbin Medical University, Harbin, China. [4]These authors contributed equally to this work. Correspondence should be addressed to H.K. (immkishi@med.u-toyama.ac.jp).

Received 2 April 2012; accepted 8 April 2013; published online 13 October 2013; doi:10.1038/nm.3358

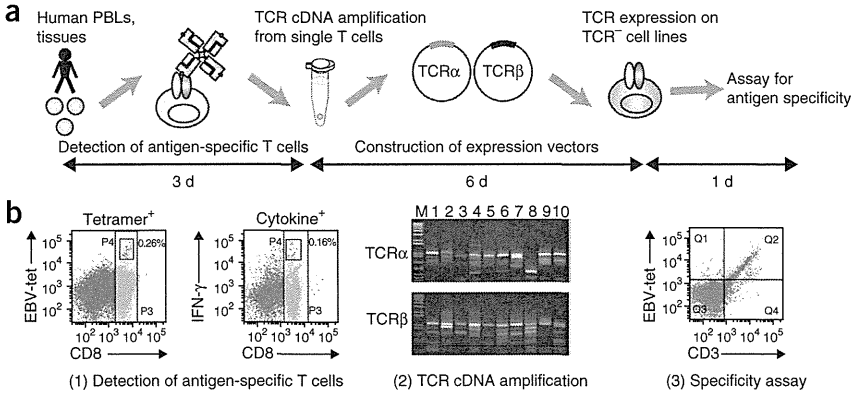

Figure 1 Schematic of the hTEC10 system. (**a**) A schematic depicting the procedure of the hTEC10 system. Briefly, human TCR cDNAs were amplified from single cells, cloned into an expression vector and then transduced into the TCR-negative T cell line TG40. The antigen specificity of TCRs was then assessed by staining the TG40 cells with MHC tetramers or by monitoring CD69 expression. The entire process can be performed within 10 d. (**b**) Detection of antigen-specific T cells with MHC tetramers (left) or cytokine secretion (right) (1), analysis of amplified TCRαβ chain cDNA (2) and examination of TCR expressed on TG40 cells using EBV tetramer (EBV-tet) binding (3).

the TCR repertoire of the tetramer-negative cells was not skewed toward a particular TCRα V or TCRβ V subgroup (**Supplementary Fig. 3**), the skewing of the TCR repertoire in the tetramer-positive cells was not due to PCR bias. Notably, our system can clone rare antigen-specific T cell clones (indicated by asterisks in **Fig. 2b** and **Supplementary Fig. 2**) that may be missed when using conventional cloning methods.

To determine the antigen specificity of the cloned TCRs, we first transferred the cDNA into TG40 cells and stained the cells with MHC-peptide tetramer mixture. The tetramer mixture bound to 95% of the cloned TCRs that were expressed on the TG40 cells (**Fig. 2c**). We then determined the antigenic peptide specificity of the cloned TCRs by stimulating the TCR-expressing TG40 cells with HLA-A24$^+$ PBLs that were pulsed with each of the EBV peptides (BRLF-1, BMLF-1, LMP2, EBNA3A or EBNA3B), followed by examining the cell-surface expression of CD69 with flow cytometry. The percentages of TCRs specific for BRLF-1, BMLF-1, EBNA3A, EBNA3B and LMP-2 among the EBV-specific TCRs were 65.5%, 12.6%, 19.7%, 1.6% and 0.5%, respectively (**Fig. 2d** and **Supplementary Table 4**).

EBV-specific TCR cDNA–transduced T cells kill target cells

To determine the cytotoxic activity of EBV-specific TCR cDNA–transduced T cells, we transduced cDNAs encoding BRLF-1–specific

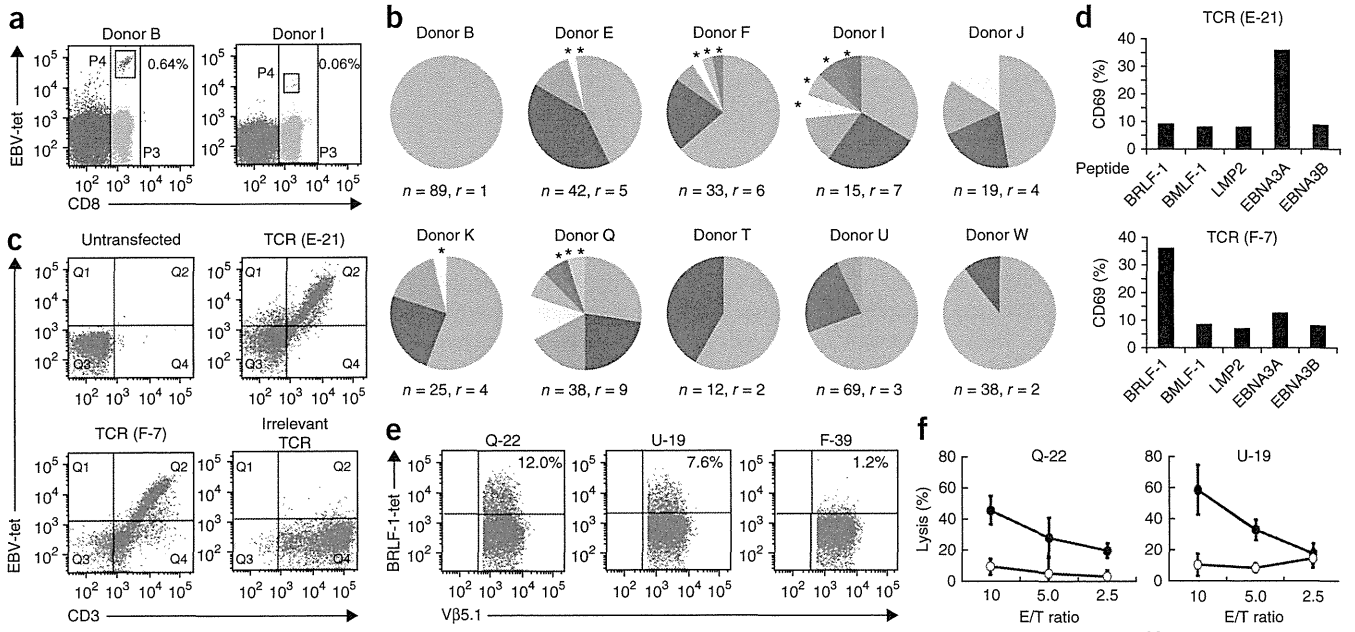

Figure 2 Analysis of EBV-specific human TCRαβ pairs obtained by hTEC10. (**a**) Flow cytometric analysis of EBV-specific CD8$^+$ T cells in human PBLs by staining with CD8-specific antibody and HLA-A*2402 EBV tetramers. Data for two out of ten donors are shown (donors B and I). The experiments were performed only once for each donor. (**b**) TCR repertoire analysis of EBV-specific CD8$^+$ T cells from ten latent healthy donors. *n*, number of analyzed T cell clones; *r*, repertoire number; asterisks, repertoire obtained from only a single T cell clone. (**c**) Determination of TCR antigen specificity by staining of TCR cDNA–transduced TG40 cells with CD3-specfic antibody and EBV tetramer mixture. Data for two TCRs out of analyzed EBV-specific TCRs are shown (E-21 and F-7 TCR). The experiments were performed twice for each TCR. (**d**) Flow cytometric analysis of CD69 expression in TG40 cells expressing E-21 or F-7 TCRs in the presence of various EBV-derived peptides and HLA-A24$^+$ PBLs. (**e**) TCR expression analysis of BRLF-1–specific Vβ5.1$^+$ TCRs (Q-22, U-19 or F-39) on TCR cDNA–transduced primary T cells by staining with Vβ5.1-specific antibody and BRLF-1–specific tetramer (BRLF-1-tet). Profile of only Vβ5.1$^+$ population is shown. The percentage of Vβ5.1 was 15.4%, 19.1% and 16.9% of PBLs for Q-22, U-19 and F-39, respectively. The percentage of tetramer-positive cells in Vβ5.1$^+$ cell population is indicated. Representative data of three independent experiments are shown. (**f**) Cytotoxicity of TCR cDNA–transduced primary T cells against T2-A24 cells pulsed with BRLF-1 peptide (closed circle) or EBNA3A peptide (open circle) labeled with calcein. The results shown are mean ± s.d. of triplicate experiments. E/T ratio, ratio of effector T cells to target cells.

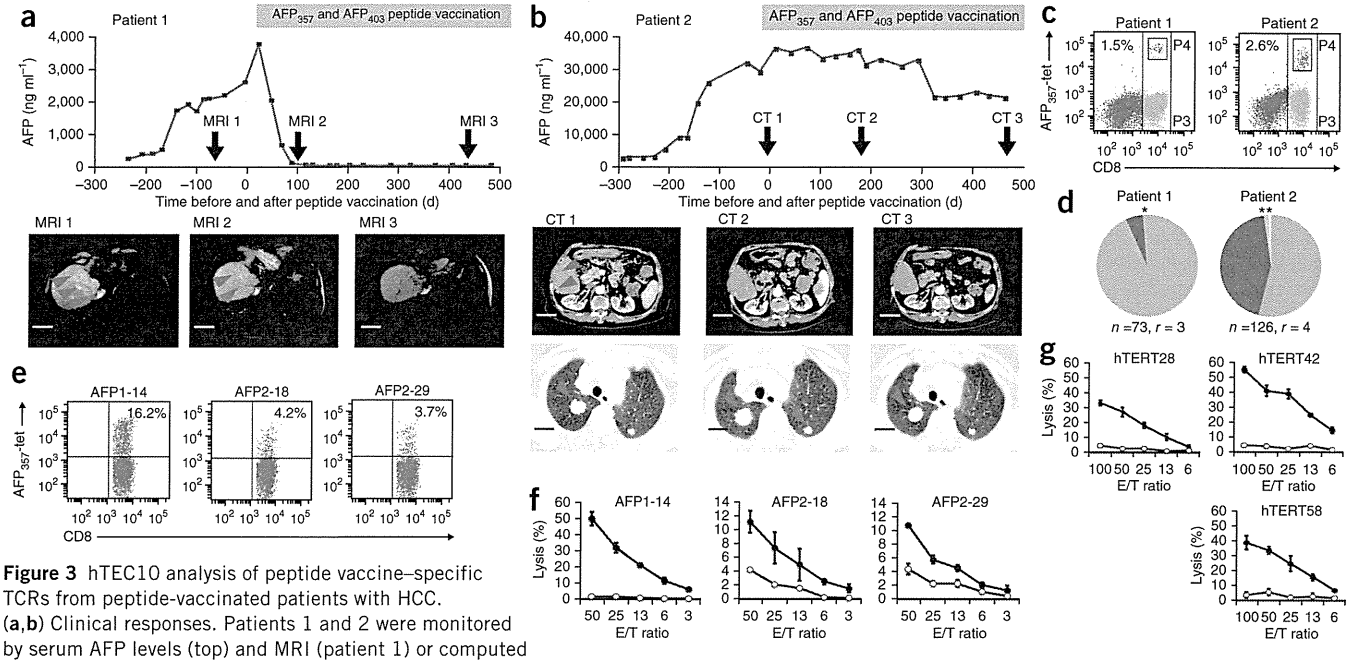

Figure 3 hTEC10 analysis of peptide vaccine–specific TCRs from peptide-vaccinated patients with HCC. (**a**,**b**) Clinical responses. Patients 1 and 2 were monitored by serum AFP levels (top) and MRI (patient 1) or computed tomography (patient 2) (bottom). Black arrows show examination dates and red arrowheads show metastatic lesions of HCC. Scale bars in **a**, 50 mm; in **b**, 50 mm (top) and 30 mm (bottom). (**c**) Detection of AFP_{357} peptide–specific $CD8^+$ T cells of PBLs in patients with HCC with CD8-specific antibody and AFP_{357}-specific tetramers. Percentages of AFP_{357}-specific tetramer-positive cells in $CD8^+$ T cells are indicated. (**d**) Repertoire of AFP_{357} $tetramer^+$ $CD8^+$ T cells. *n*, number of analyzed T cell clones; *r*, repertoire number; asterisk, repertoire obtained from only a single T cell clone. (**e**) Expression of AFP_{357}-specific TCRs on TCR cDNA–transduced primary T cells. Profile of only $CD8^+$ population is shown. Percentages of AFP_{357}-specific tetramer-positive cells among $CD8^+$ T cells are indicated. (**f**) Cytotoxicity of AFP-specific TCR cDNA–transduced primary T cells toward C1R-A24 cells pulsed with AFP_{357}-peptide (closed circle) or control peptide (open circle). Data are expressed as mean ± s.d. of triplicate experiments. Representative data of three independent experiments are shown. (**g**) Cytotoxicity of hTERT–specific TCR cDNA–transduced primary T cells toward C1R-A24 cells pulsed with $hTERT_{461}$ peptide (closed circle) or control peptide (open circle). Data are expressed as mean ± s.d. of triplicate experiments. Representative data of three independent experiments are shown.

$V\beta5.1^+$ TCRs (clones Q-22, U-19 and F-39) into primary human T cells using retroviral vectors and compared their ability to kill T2-A24 cells, a TAP-deficient T2 cell line expressing HLA-A*2402 (ref. 8), that had been pulsed with the BRLF-1 peptide. These three TCRs have the same Vβ region ($V\beta5.1^+$) but distinct CDR3 sequences and Vα regions. The BRLF-1 tetramer bound to 12.0%, 7.6% and 1.2% of $V\beta5.1^+$ cells in the T cell populations that were transduced with Q-22, U-19 and F-39 TCR cDNAs, respectively, whereas the percentages of $V\beta5.1^+$ cells in the Q-22, U-19 and F-39 TCR cDNA transfectants were the same level (**Fig. 2e** and **Supplementary Fig. 4a**). This result indicates that the transduced TCRs tend to mispair with endogenous TCRs[9].

We then determined the cytotoxic activity of T cells that were transduced with the BRLF-1–specific TCR cDNAs against T2-A24 cells that had been pulsed with the BRLF-1 or the EBNA3A peptide. T cells transduced with BRLF-1–specific TCR cDNAs exhibited cytotoxicity toward the BRLF-1 peptide–pulsed T2-A24 cells but not toward the EBNA3A peptide–pulsed cells (**Fig. 2f**), demonstrating that the cytotoxic activity was peptide specific. Similarly, T cells transduced with EBNA3A-specific TCR (E-21) cDNAs demonstrated cytotoxicity toward EBNA3A peptide–pulsed T2-A24 cells but not BRLF-1 peptide–pulsed cells (**Supplementary Fig. 5a**,**c**).

We also measured the cytokine secretion of the TCR cDNA–transduced T cells after antigen stimulation. Peripheral blood lymphocytes (PBLs) transduced with BRLF-1–specific TCR cDNAs (Q-22, U-19 and F-39) secreted multiple cytokines (interferon-γ (IFN-γ), tumor necrosis factor-α (TNF-α) and interleukin-2 (IL-2)) upon stimulation with the BRLF-1 peptide, but not with the EBNA3A peptide (**Supplementary Fig. 6**). In contrast, PBLs transduced with the EBNA3A-specific TCR (E-21) cDNAs secreted IFN-γ upon stimulation with the EBNA3A peptide but with the BRLF-1 peptide (**Supplementary Fig. 5b**).

Furthermore, we examined the functional avidity of the EBV-specific TCRs using the TG40-based TCR downregulation assay, and we determined the half-maximum inhibitory concentration (IC_{50}) of the peptide responses. The Q-22 TCR exhibited the highest functional avidity (**Supplementary Fig. 7** and **Supplementary Table 5**). Therefore, we examined whether T cells transduced with the Q-22 TCR cDNA could respond to EBV-transformed lymphoblastoid cell line (LCL) cells endogenously expressing the EBV antigen and HLA-A*2402 (JTK-LCL cells). The Q-22 TCR cDNA–transduced T cells exhibited a marked response to JTK-LCL cells and produced IFN-γ (**Supplementary Fig. 8**). However, we did not detect CTL activity of the Q-22 TCR cDNA–transduced T cells against JTK-LCL cells. These data are in agreement with a previous report[7]. This lack of cytotoxicity may be owing to limited presentation of the BRLF-1 peptide by HLA-A*2402 on the cell surface of JTK-LCL cells.

In summary, we obtained 380 EBV-specific TCRαβ cDNA pairs and analyzed the TCR repertoires. All of the cloned TCRs were previously uncharacterized (**Supplementary Table 6**).

Clinical application of hTEC10 system in people with cancer

To apply the hTEC10 system to patients with cancer, we obtained PBLs from two patients with hepatocellular carcinoma (HCC) who had been treated with α-fetoprotein (AFP)-derived peptide vaccines and exhibited clinical responses. We show the clinical courses of cancer in these patients (**Fig. 3a**,**b**). The first patient (patient 1), who was infected with hepatitis B virus (HBV) and had a large HCC tumor with vascular invasion of

the portal vein, was vaccinated with the AFP_{357} and AFP_{403} peptides biweekly for 72 weeks. After vaccination, the patient's elevated serum AFP value was normalized; the size of the HCC tumor also decreased, and it eventually disappeared, as evaluated by magnetic resonance imaging (MRI) (**Fig. 3a**), indicating a complete response. The second patient (patient 2), who was infected with HBV and had multiple metastatic HCC lesions in the abdominal wall and lungs, was vaccinated with the AFP_{357} and AFP_{403} peptides biweekly for 88 weeks. After vaccination, the patient's elevated serum AFP value decreased, and the metastatic HCC lesions in the abdominal wall disappeared, as evaluated by computed tomography (**Fig. 3b**). The size and number of lung metastases did not change over the 88 weeks of treatment, indicating stable disease.

We examined whether AFP_{357}-specific T cells could be detected in the PBLs of patients 1 and 2 before or during vaccination by employing an AFP_{357}-specific tetramer and flow cytometry. We could not detect AFP-specific $CD8^+$ T cells detected in the PBLs of the patients either before or during treatment (**Supplementary Fig. 9**). However, when we incubated the PBLs with AFP-derived peptides for 3 weeks to expand the AFP-specific $CD8^+$ T cells, we detected AFP_{357}-specific T cells in the PBLs obtained from both patients during vaccination but not from the PBLs obtained before vaccination (**Supplementary Fig. 10**). These data indicate that the detection of AFP_{357}-specific TCRs in the patients' PBLs was due to peptide vaccination.

1.5% and 2.6% of the $CD8^+$ T cells were positive for tetramer staining in patients 1 and 2, respectively (**Fig. 3c**). We then sorted the single AFP tetramer–positive $CD8^+$ T cells, amplified the TCR cDNAs and analyzed their sequences. We obtained 73 and 126 AFP-specific TCRs from patients 1 and 2, respectively. The sequence analysis revealed that the hTEC10 system yielded three and four T cell clones from patients 1 and 2, respectively (**Fig. 3d**), suggesting that peptide vaccination induced the oligoclonal expansion of AFP-specific T cells in these patients. Alternatively, *in vitro* culture may have resulted in the oligoclonal expansion of AFP-specific T cells. In contrast to EBV-specific TCRs, the repertoires of AFP-specific TCRs might be biased by *in vitro* culture, as suggested by Zhou *et al.*[10]. Notably, the hTEC10 system could clone TCRs from very rare antigen-specific T cells, as in the case of EBV-specific minor clones (**Fig. 3d**).

We then transduced three of the obtained AFP-specific TCR cDNAs into primary T cells of a healthy donor and analyzed the binding of the AFP tetramer. The TCR cDNAs were transduced into 28–32% of the T cells (**Supplementary Fig. 4b**), and 3.7–16.2% of the total $CD8^+$ cells bound the AFP tetramer (**Fig. 3e**). We then determined the cytotoxic activity of the transduced T cells toward C1R-A24 cells (an LCL transfected with HLA-A*2402)[11] pulsed with the AFP peptide. The T cells transduced with these TCR cDNAs showed marked cytotoxicity toward AFP peptide–pulsed C1R-A24 cells but not control peptide ($HIV_{584-592}$)-pulsed cells (**Fig. 3f**), indicating that the cytotoxic activity was peptide specific. We also measured cytokine secretion by the TCR cDNA–transduced T cells after antigen stimulation. PBLs transduced with AFP_{357}-specific TCR cDNAs (AFP1-14, AFP2-28 and AFP2-29), but not PBLs transduced with control GFP vector, secreted IFN-γ when stimulated with the AFP_{357} peptide (**Supplementary Fig. 11**).

Next, we examined the cytotoxic activity of the T cells transduced with AFP-specific TCR cDNAs to HepG2 cells, which endogenously express AFP[11]. However, they did not show any specific cytotoxicity to the target cells (data not shown). We also obtained four kinds of human telomerase reverse transcriptase (hTERT)-specific TCRs from patients with HCC who had been vaccinated with hTERT peptide in the clinical trial (**Supplementary Fig. 12**). We transduced three hTERT-specific TCR cDNAs in primary T cells and examined their cytotoxic activity toward

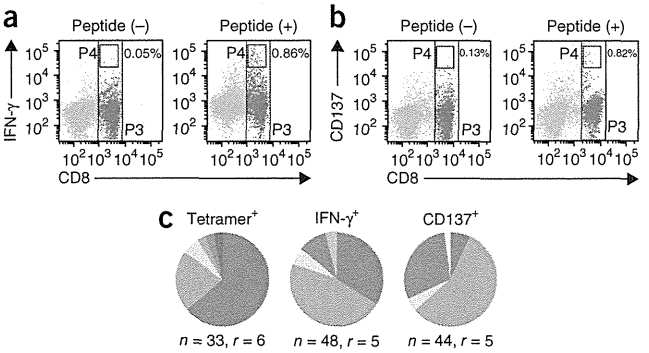

Figure 4 Repertoire analysis of cytokine-secreting $CD8^+$ T cells by stimulation with a specific peptide. (**a**) Secretion of IFN-γ by BRLF-1 peptide–stimulated PBLs. Percentages of IFN-γ–secreting cells in $CD8^+$ T cells are indicated. (**b**) Upregulation of CD137 on BRLF-1 peptide–stimulated PBLs. (**c**) Repertoires of IFN-γ$^+$ $CD8^+$ T cells and $CD137^+$ $CD8^+$ T cells. *n*, number of analyzed T cell clones; *r*, repertoire number. The same color denotes the same Vα or Vβ repertoires.

hTERT peptide–pulsed C1R-A24 cells or HepG2 cells that endogenously expressed hTERT. The T cells transduced with human TERT–specific TCR cDNAs (hTERT28, hTERT42 and hTERT58) showed marked cytotoxicity toward hTERT peptide–pulsed C1R-A24 cells (**Fig. 3g**). However, they did not show marked cytotoxicity toward HepG2 cells (data not shown). These results demonstrate that the hTEC10 system can clone functional TAA peptide–specific TCRs from patients with cancer.

Improvement of the hTEC10 system

We next established new MHC tetramer-independent systems to clone TCR cDNAs using cytokine secretion and CD137 upregulation. We obtained PBLs from healthy donors with latent EBV infection and incubated these cells with the BRLF-1 peptide to expand the BRLF-1–specific $CD8^+$ T cells *in vitro*. We then stimulated the expanded BRLF-1–specific $CD8^+$ T cells in the presence of CD28-specific antibody with or without the BRLF-1 peptide and examined IFN-γ secretion or CD137 upregulation. 0.86% of the $CD8^+$ T cells were IFN-γ positive, and 0.82% of the $CD8^+$ T cells had upregulated CD137 (**Fig. 4a,b**). We then sorted the single T cells and analyzed their TCR sequences. We obtained 48 TCRs from the IFN-γ–secreting cells and 44 TCRs from the CD137-upregulated cells, and we compared the repertoires of these populations with those obtained from the MHC-peptide tetramer staining method (**Fig. 4c**).

We found that 86% of the TCR repertoire of the IFN-γ–positive T cells and 68% of that for the CD137-upregulated T-cells was identical to that identified by staining with the MHC-peptide tetramer. We also tested the tetramer-binding ability of five TCR clones that were isolated with the IFN-γ–based protocol and five TCR clones that were isolated with the CD137 upregulation protocol. All of the clones bound the tetramer (data not shown). In addition, we examined the ability of six TCRs that bound the MHC-peptide tetramer (**Supplementary Fig. 13**) to induce IFN-γ production when transduced into PBLs. All six TCR cDNA–transduced PBLs produced IFN-γ (**Supplementary Fig. 14**). Taken together, these results demonstrate that the hTEC10 system can rapidly and efficiently clone TCR cDNAs by assessing cytokine secretion or CD137 upregulation.

DISCUSSION

In this study, we established a system for the rapid and direct cloning and functional evaluation of TCR cDNAs derived from single antigen-specific

human T cells (hTEC10 system). We used this system to obtain and analyze antigen-specific TCRs from healthy donors and patients with cancer.

With regard to minimal frequencies of specific T cells required for the proper identification of TCRs, the frequency of the EBV tetramer$^+$ cells of donor I was the minimum (0.06% of the CD8$^+$ T cells or 0.01% of the total PBLs). We sorted 48 EBV tetramer$^+$ cells from 8×10^6 cells. Twenty-three pairs of TCR α and β cDNAs were amplified. Fifteen of them could be expressed in TG40 cells and could bind EBV tetramer.

Regarding the processing time, the hTEC10 system can obtain antigen-specific TCR cDNAs within 10 d when the antigen-specific T cells are detected on day 1. If the antigen-specific T cells cannot be detected in primary T cells, they need to be cultured for a certain duration. Thus, 8 d, plus additional days for *in vitro* culture, are required to obtain antigen-specific TCRs.

Concerning the EBV-specific TCR repertoires, all of the cloned TCRs were previously uncharacterized. The repertoire of EBV-specific TCRs was highly restricted, in agreement with previous reports[12,13]. The analysis was reproducible, as we obtained similar results from donor B and donor E in two independent experiments.

To determine candidate TCRs for gene therapy for cancer, we used the hTEC10 system to analyze PBLs derived from patients with HCC who had been successfully treated by AFP-derived peptide vaccination. The appropriateness of oncofetal antigens as targets for TCR gene therapy has recently been questioned[14]. However, Butterfield *et al.*[15] previously reported that a phase 1/2 clinical trial of immunization with dendritic cells pulsed with HLA-A*0201–restricted AFP peptides in patients with HCC showed no adverse events. Furthermore, we previously compared the *in vitro* effect of various TAA peptides on PBLs from patients with HCC and showed that HLA-A*2402–restricted AFP peptides may be candidates for peptide vaccination of patients with HCC[11,16]. Thus, a clinical trial to determine the effectiveness of AFP-derived peptide vaccination for patients with HCC has already been conducted, and several patients have exhibited positive clinical responses.

Our data showed that primary T cells transduced with AFP-specific and hTERT-specific TCR cDNAs showed potent antigen-specific cytotoxicity toward AFP- or hTERTpeptide–pulsed target cells, but they did not show marked cytotoxicity toward HepG2 cells that had been reported to endogenously express AFP and hTERT (data not shown). We reasoned three possibilities. The first is that the efficiencies of TCR transduction into PBLs were low. The second is that HepG2 cells may present an insufficient amount of hTERT peptide on their HLA-A24 molecules. The third is the weak affinity of the obtained TCRs. We need to clone more AFP- and hTERT-specific TCRs to acquire TCRs with sufficient affinity to induce cytotoxicity toward HepG2 cells.

Finally, we applied the hTEC10 system to detect and retrieve TCRαβ pair cDNAs by analyzing cytokine secretion and CD137 upregulation. Most of the TCR repertoire of IFN-γ–positive T cells or CD137-upregulated T cells was identical to that identified by the MHC-peptide tetramer, whereas the rest were not identical. These results, along with the CD69 induction assay, indicate that the hTEC10 system can be used with cytokine-secreting or CD137-upregulated CD8$^+$ T cells without the need for staining with an MHC-peptide multimer. Therefore, we can apply the hTEC10 system to isolate T cells from patients with cancer for whom the identity of the tumor antigen is unknown. The T cells can be stimulated with tumor cells, and the IFN-γ–secreting or CD137-upregulated CD8$^+$ cells can be sorted. After cloning the TCRs, their specificity can be examined by analyzing the response of TCR cDNA–transduced T cells to the tumor cells.

METHODS

Methods and any associated references are available in the online version of the paper.

Accession codes. cDNA sequences were deposited in DNA Data Bank of Japan with accession codes from AB749820 to AB749925.

Note: Any Supplementary Information and Source Data files are available in the online version of the paper.

ACKNOWLEDGMENTS

We thank S. Hirota, A. Takishita, K. Shitaoka and M. Horii for technical assistance and K. Hata for secretarial work. This research was supported by grants from the Hokuriku Innovation Cluster for Health Science and a Grant-in-Aid from the Ministry of Education, Culture, Sports, Science and Technology in Japan (11F01415 and 24650630). Retroviral pMX vector, pMX-IRES-EGFP vector and PLAT-E cell line were kindly provided by T. Kitamura (University of Tokyo), human CD8–expressing TG40 cell line by T. Ueno and C. Motozono (Kumamoto University) with permission from T. Saito (Riken), T2-A24 cell line by K. Kuzushima (Aichi Cancer Center Research Institute), Phoenix-A cell line by G. Nolan (Stanford University) and C1R-A24 cell line from M. Takiguchi (Kumamoto University).

AUTHOR CONTRIBUTIONS

E.K., E.M., H.H., T.N. and A.J. performed and analyzed the experiments. E.K., E.M., H.K., S.K., H.N. and A.M. designed the experiments. E.M. and T.O. contributed reagents. E.K., H.K. and A.M. wrote the manuscript, and E.K., E.M., H.K., S.K. and A.M. edited the manuscript.

COMPETING FINANCIAL INTERESTS

The authors declare no competing financial interests.

1. Morgan, R.A. *et al.* Cancer regression in patients after transfer of genetically engineered lymphocytes. *Science* **314**, 126–129 (2006).
2. Johnson, L.A. *et al.* Gene therapy with human and mouse T-cell receptors mediates cancer regression and targets normal tissues expressing cognate antigen. *Blood* **114**, 535–546 (2009).
3. Linnemann, C., Schumacher, T.N. & Bendle, G.M. T-cell receptor gene therapy: critical parameters for clinical success. *J. Invest. Dermatol.* **131**, 1806–1816 (2011).
4. Uttenthal, B.J., Chua, I., Morris, E.C. & Stauss, H.J. Challenges in T cell receptor gene therapy. *J. Gene Med.* **14**, 386–399 (2012).
5. Ozawa, T., Tajiri, K., Kishi, H. & Muraguchi, A. Comprehensive analysis of the functional TCR repertoire at the single-cell level. *Biochem. Biophys. Res. Commun.* **367**, 820–825 (2008).
6. Dash, P. *et al.* Paired analysis of TCRα and TCRβ chains at the single-cell level in mice. *J. Clin. Invest.* **121**, 288–295 (2011).
7. Kuzushima, K. *et al.* Tetramer-assisted identification and characterization of epitopes recognized by HLA A*2402-restricted Epstein-Barr virus-specific CD8$^+$ T cells. *Blood* **101**, 1460–1468 (2003).
8. Miyahara, Y. *et al.* Determination of cellularly processed HLA-A2402–restricted novel CTL epitopes derived from two cancer germ line genes, MAGE-A4 and SAGE. *Clin. Cancer Res.* **11**, 5581–5589 (2005).
9. Okamoto, S. *et al.* Improved expression and reactivity of transduced tumor-specific TCRs in human lymphocytes by specific silencing of endogenous TCR. *Cancer Res.* **69**, 9003–9011 (2009).
10. Zhou, J., Dudley, M.E., Rosenberg, S.A. & Robbins, P.F. Selective growth, *in vitro* and *in vivo*, of individual T cell clones from tumor-infiltrating lymphocytes obtained from patients with melanoma. *J. Immunol.* **173**, 7622–7629 (2004).
11. Mizukoshi, E., Nakamoto, Y., Tsuji, H., Yamashita, T. & Kaneko, S. Identification of α-fetoprotein–derived peptides recognized by cytotoxic T lymphocytes in HLA-A24$^+$ patients with hepatocellular carcinoma. *Int. J. Cancer* **118**, 1194–1204 (2006).
12. Lim, A. *et al.* Frequent contribution of T cell clonotypes with public TCR features to the chronic response against a dominant EBV-derived epitope: application to direct detection of their molecular imprint on the human peripheral T cell repertoire. *J. Immunol.* **165**, 2001–2011 (2000).
13. Argaet, V.P. *et al.* Dominant selection of an invariant T cell antigen receptor in response to persistent infection by Epstein-Barr virus. *J. Exp. Med.* **180**, 2335–2340 (1994).
14. Parkhurst, M.R. *et al.* T cells targeting carcinoembryonic antigen can mediate regression of metastatic colorectal cancer but induce severe transient colitis. *Mol. Ther.* **19**, 620–626 (2011).
15. Butterfield, L.H. *et al.* A phase I/II trial testing immunization of hepatocellular carcinoma patients with dendritic cells pulsed with four α-fetoprotein peptides. *Clin. Cancer Res.* **12**, 2817–2825 (2006).
16. Mizukoshi, E. *et al.* Comparative analysis of various tumor-associated antigen-specific T-cell responses in patients with hepatocellular carcinoma. *Hepatology* **53**, 1206–1216 (2011).

ONLINE METHODS

Healthy donors and human leukocyte antigen typing. Human experiments were performed with the approval of the Ethical Committee at the University of Toyama, Toyama, Japan. Informed consent was obtained from all subjects. PBLs were isolated as described previously[16]. HLA-A24 and HLA-A02 haplotype positivity was screened by staining PBLs with FITC-conjugated HLA-A24 (clone 17A10) and HLA-A2 (clone BB7.2) antibody (MBL) and analyzed with flow cytometry.

Peptide vaccination of patients. The clinical trial of the HLA-A24–restricted AFP_{357} (EYSRRHPQL) and AFP_{403} (KYIQESQAL) peptide vaccines (trial registration: UMIN000003514) and that of the HLA-A24–restricted $hTERT_{461}$ (VYGFVRACL) peptide vaccines (trial registration: UMIN000003511) were conducted at Kanazawa University Hospital, Kanazawa, Japan. Patients with verified radiological diagnoses of HCC stage III or IV were enrolled in this study. The patients each received 3.0 mg of AFP-derived peptide vaccine in each dose. The peptides, which were synthesized as GMP-grade products at Neo MPS, were administered as an emulsified solution containing incomplete Freund's adjuvant (Montanide ISA-51 VG; SEPPIC) by biweekly subcutaneous immunization for 72 weeks (patient 1) and 88 weeks (patient 2). Clinical responses were monitored by measuring the serum AFP value and carrying out dynamic computed tomography or MRI and were evaluated according to the Response Evaluation Criteria in Solid Tumors, version 1.1. All patients provided written informed consent to participate in the study in accordance with the Helsinki Declaration, and this study was approved by the regional ethics committee (Medical Ethics Committee of Kanazawa University, No. 858). Blood samples from the patients were tested for the surface antigen of the HBV and hepatitis C virus using commercial immunoassays (Fuji Rebio). HLA-based typing of patient PBLs was performed using the polymerase chain reaction–reverse sequence-specific oligonucleotide (PCR-RSSO) method. The serum AFP level was measured by ELISA (Abbott Japan). PBLs were isolated from patients as described previously[16], resuspended in RPMI 1640 medium containing 80% FCS and 10% dimethyl sulfoxide and cryopreserved until use.

Cell culture and cell lines. RPMI 1640 and DMEM media (Wako Pure Chemical) were supplemented with 10% FBS (Biowest), 100 μg ml^{-1} streptomycin and 100 U ml^{-1} penicillin. Human CD8–expressing TG40 cells[17], T2-A24 cells[8] from a transporter associated with antigen presentation (TAP)-deficient T2 cell line transfected with HLA-A*2402 and C1R-A24 cells from a C1R lymphoblastoid cell line transfected with HLA-A*2402 (ref. 11) were maintained in RPMI 1640 medium. PLAT-E[18] and Phoenix-A[19] (a retroviral packaging cell line) and HepG2, (hepatocellular carcinoma cell line, purchased from ATCC), were maintained in DMEM medium.

Antibody and MHC tetramer staining. FITC-conjugated CD8-specific antibody (1: 200, clone T8) and PC5-conjugated CD8-specific antibody (1: 1,000, clone B9.11) were purchased from Beckman Coulter. Phycoerythrin-conjugated CD137-specific antibody (1:40, clone 4B4-1) was purchased from BioLegend. Biotin-conjugated CD3ε-specific antibody (1:200, clone 145-2C11), allophycocyanin-conjugated streptavidin and phycoerythrin-conjugated CD69-specific antibody (1:200, clone H1.2F3) were purchased from eBioscience. EBV-specific T cells were stained with phycoerythrin-conjugated HLA-A*2402–peptide tetramers or HLA-A*0201–peptide tetramers. The sequences of the HLA-A*2402-restricted EBV peptides are as follows: TYPVLEEMF (BRLF-$1_{198-206}$), DYNFVKQLF (BMLF-$1_{320-328}$), IYVLVMLVL (LMP$2_{222-230}$), RYSIFFDYM (EBNA$3A_{246-254}$) and TYSAGIVQI (EBNA$3B_{217-225}$). The sequences of the HLA-A*0201-restricted EBV peptides are GLCTLVAML (BMLF-$1_{280-288}$) and YLQQNWWTL (LMP$1_{159-167}$). AFP-specific or hTERT-specific T cells were stained with the phycoerythrin-conjugated HLA-A*2402 peptide ($AFP_{357-365}$)[11] or HLA-A*2402 peptide ($hTERT_{461-469}$)[20]. All tetramers were purchased from MBL.

Single-cell sorting and RT-PCR. Tetramer-positive cells that had been stimulated with IL-2 and phytohemagglutin for 2 d were single-cell–sorted by FACSAria (Becton Dickinson) into MicroAmp reaction tubes (Applied Biosystems) that contained a cell lysis solution composed of 29.2 μg Dynabeads Oligo$(dT)_{25}$ (Invitrogen), 2.9 μl Lysis/Binding Buffer (Invitrogen) and 0.29 pmol of each gene-specific primer. The sequences of the primers were as follows: alpha-RT 5′-AGCAGTGTTTGGCAGCT CTT-3′, beta1-RT 5′-CTGGCAAAAGAAGAATGTGT-3′ and beta2-RT (5′-ACACAGATTGGGAGCAGGTA-3′). The Dynabeads were then transferred into a solution containing 4.0 U SuperScriptIII (Invitrogen), 0.3 U Murine RNase inhibitor (New England BioLabs), 0.5 mM each dNTP, 5 mM DTT, 0.2% Triton X-100 and 1× First-Strand Buffer (Invitrogen). The reverse transcription reaction was performed for 40 min at 50 °C. After the reverse transcription reaction, the Dynabeads were transferred into another solution containing 8 U of terminal deoxynucleotidyl transferase (Roche), 0.5 mM dGTP, 0.4 U murine RNase inhibitor, 4 mM $MgCl_2$, 0.2% Triton X-100, 50 μM K_2HPO_4 and 50 μM KH2PO4, pH 7.0, and were incubated for 40 min at 37 °C to add a poly-dG tail to the 3′ end of the cDNA. The Dynabeads were then transferred into a new PCR tube containing the first PCR reaction mixture. The first PCR was performed using PrimeSTAR HS DNA polymerase (TaKaRa) according to the manufacturer's instructions with the AP-1, alpha-1st, beta1-1st and beta2-1st primers. The PCR cycles for AP-1 (5′-ACAGCAGGTCAGTCAAGCAGTAGCAGCAGTTCG ATAACTTCGAATTCTGCAGTCGACGGTACCGCGGGCCCGGGATC CCCCCCCCCCCDN-3′), alpha-1st (5′-AGAGGGAGAAGAGGGGCA AT-3′), beta1-1st (5′-CCATGACGGGTTAGAAGCTC-3′) and beta2-1st (5′-GGATGAAGAATGACCTGGGAT-3′) were as follows: 5 min at 95 °C followed by 30 cycles of 15 s at 95 °C, 5 s at 60 °C and 1 min 30 s at 72 °C.

The resultant PCR mixtures were diluted 100-fold with water, and 2 μl of the diluted PCR mixtures were added to 23 μl of the nested PCR mixture as template DNA. The nested PCR was performed in a reaction mixture similar to that for the first PCR but with the adaptor primer AP-2 (5′-AGCAGTAGCAGCAGTTCGATAA-3′) and a primer specific for the constant region of TCRα (alpha-nest, 5′-GGTGAATAGGCAGACAGACTT-3′) or TCRβ (beta-nest, 5′-GTGGCCAGGCACACCAGTGT-3′). The PCR cycles were as follows: 1 min at 98 °C followed by 35 cycles of 15 s at 98 °C, 5 s at 60 °C and 45 s at 72 °C.

The PCR products were then analyzed with the alpha-nest or beta-nest primer by either direct sequencing or sequencing after subcloning into an expression vector. The TCR repertoire was analyzed with the IMGT/V-Quest tool (http://www.imgt.org/)[21].

Retroviral transfection. The cDNAs encoding the TCRα or TCRβ chain were independently inserted into a pMX vector or pMX-IRES-EGFP vector[22], which was then transfected into PLAT-E cells with FuGENE 6 (Roche). The culture supernatant was collected 72 h after transfection and added to human CD8–TG40 cells together with polybrene (Sigma-Aldrich). EBV-specific tetramer binding was analyzed by flow cytometry. For transduction into human PBLs, the TCRα and TCRβ chains were linked by a viral F2A sequence[23] or a P2A sequence[24], cloned into the pMX-IRES-EGFP vector and transfected into the Phoenix A cells. Transduction efficiency was monitored by the expression of EGFP.

Determination of the antigen specificity of cloned TCRs. The antigen specificity of the cloned TCRαβ pairs was analyzed using the CD69 induction assay, tetramer staining or both. Briefly, TCR-expressing human CD8–TG40 cells were incubated overnight with HLA-A24$^+$ PBLs in the presence of each of the EBV peptides (BRLF-1, BMLF-1, LMP2, EBNA3A or EBNA3B). After incubation, the cell surface expression of CD69 was analyzed by flow cytometry.

Preparation of PBLs transduced with cloned TCR cDNAs. 5×10^5 PBLs were stimulated *in vitro* with CD3/CD28 Dynabeads (Invitrogen) and 30 IU ml^{-1} recombinant hIL-2 (Peprotech) according to the manufacturer's instructions. On day 2, the stimulated PBLs were washed, and 5×10^5 cells were resuspended in the medium containing 30 IU ml^{-1} recombinant hIL-2. The cells were added to each well in the plates that had been coated with 50 μg ml^{-1} retronectin (TaKaRa) and spin-loaded with TCR-encoding retroviral supernatant by centrifuging for 2 h at 1,900*g* at 32 °C. The cells were spun down at 1,000*g* at 32 °C for 10 min and incubated overnight at 37 °C in 5% CO_2. On day 3, the PBLs were transferred onto newly prepared retroviral-coated plates

as on day 2 and cultured with 30 IU ml^{-1} recombinant hIL-2. On day 10, the TCR cDNA–transduced PBLs were evaluated for expression of the appropriate TCR by tetramer staining and flow cytometry.

Cytotoxic T lymphocyte assay. In the case of the AFP-specific and hTERT-specific TCRs, the cytotoxicity of the TCR cDNA–transduced PBLs was measured by the ^{51}chromium release assay[11]. In the case of the EBV-specific TCR, the cytotoxicity of the TCR cDNA–transduced PBLs was measured using the calcein-AM (Wako Pure Chemical) release assay. Briefly, peptide-loaded T2-A24 target cells were labeled with 25 μM calcein-AM for 30 min at 37 °C. Then, the target cells and TCR cDNA–transduced PBLs (effector cells) were plated in 96-well plates at the indicated effector-to-target (E/T) ratios and incubated for 4 h. After incubation, the fluorescence of calcein in the supernatants was measured using FLUOstar OPTIMA microplate reader (BMG LABTECH). The percentage of cytotoxicity was calculated using the following formula: % lysis = (F experiment − F spontaneous)/(F maximal − F spontaneous) × 100.

IFN-γ secretion assay. IFN-γ–secreting cells were detected using the IFN-γ secretion assay (Miltenyi Biotec) according to the manufacturer's instructions. Briefly, PBLs were stimulated with the BRLF-1 peptide for 14 d. After *in vitro* stimulation, the PBLs were stimulated with CD28-specific antibody with or without the BRLF-1-peptide for 6 h. The PBLs were washed and stained with IFN-γ Catch Reagent (Miltenyi Biotec). The PBLs were then suspended in 1 ml medium and incubated for 45 min to allow cytokine secretion. After washing, the PBLs were stained with phycoerythrin-conjugated IFN-γ Detection Reagent (Miltenyi Biotec) and FITC-conjugated CD8-specific antibody.

ELISA assay. ELISA assays were performed according to the manufacturer's instructions. Briefly, 1×10^5 TCR cDNA–transduced PBLs were cocultured with 1×10^5 T2-A24 cells pulsed with specific peptide. After 16 h incubation, the supernatants were collected, and IFN-γ, IL-2 and TNF-α in the supernatant were measured by ELISA (R&D systems). The results shown are the mean ± s.d. of triplicate experiments.

TG40-based TCR downregulation assay. The IC_{50} of the peptide responses of the TCRαβ cDNA–transduced TG40 was determined with TCR downregulation assay[7]. Briefly, human CD8-TG40 cells expressing TCRs specific for BRLF-1 were incubated overnight with T2-A24 cells in the presence of various concentrations of BRLF-1 peptide. After incubation, the CD3ε expression was analyzed by flow cytometry. The percentage of CD3ε expression was calculated using the following formula: % CD3ε expression = (CD3ε expression in the presence of indicated concentration of specific peptide)/(CD3ε expression in the absence of specific peptide) × 100. The IC_{50} values were calculated by probit analysis[25].

ELISPOT assay. IFN-γ ELISPOT assays were performed as previously reported[26]. 96-well multiscreen filter plates (Millipore) were coated with 5 μg ml^{-1} human IFN-γ–specific antibody (catalog number DY285, R&D Systems) and blocked with culture medium. Then, EBV-transformed JTL-LCL cells with or without HLA-ABC–specific antibody (clone B9.12.1) (Beckman Coulter) were plated with TCR cDNA–transduced PBLs at the indicated cell numbers and incubated for the indicated times. After incubation, 1 μg ml^{-1} biotin-conjugated human IFN-γ–specific antibody (catalog number BAF285, R&D systems) was added, followed by alkaline phosphatase–conjugated streptavidin (Sigma). After washing, a mixture of 3-bromo-4-chloro-3-indolyl-phosphate toluidine and *p*-nitroblue tetrazolium chloride (Sigma) was added to detect the immunospots.

17. Ueno, T., Tomiyama, H., Fujiwara, M., Oka, S. & Takiguchi, M. Functionally impaired HIV-specific CD8 T cells show high affinity TCR-ligand interactions. *J. Immunol.* **173**, 5451–5457 (2004).
18. Morita, S., Kojima, T. & Kitamura, T. Plat-E: an efficient and stable system for transient packaging of retroviruses. *Gene Ther.* **7**, 1063–1066 (2000).
19. Kinsella, T.M. & Nolan, G.P. Episomal vectors rapidly and stably produce high-titer recombinant retrovirus. *Hum. Gene Ther.* **7**, 1405–1413 (1996).
20. Mizukoshi, E. *et al.* Cytotoxic T cell responses to human telomerase reverse transcriptase in patients with hepatocellular carcinoma. *Hepatology* **43**, 1284–1294 (2006).
21. Giudicelli, V., Chaume, D. & Lefranc, M.P. IMGT/V-QUEST, an integrated software program for immunoglobulin and T cell receptor V-J and V-D-J rearrangement analysis. *Nucleic Acids Res.* **32**, W435–W440 (2004).
22. Onishi, M. *et al.* Applications of retrovirus-mediated expression cloning. *Exp. Hematol.* **24**, 324–329 (1996).
23. Ryan, M.D., King, A.M. & Thomas, G.P. Cleavage of foot-and-mouth disease virus polyprotein is mediated by residues located within a 19 amino acid sequence. *J. Gen. Virol.* **72**, 2727–2732 (1991).
24. Leisegang, M. *et al.* Enhanced functionality of T cell receptor-redirected T cells is defined by the transgene cassette. *J. Mol. Med. (Berl)* **86**, 573–583 (2008).
25. Goldstein, A. *Biostatistics: An Introductory Text* (Macmillan, New York, 1964).
26. Jin, A. *et al.* A rapid and efficient single-cell manipulation method for screening antigen-specific antibody-secreting cells from human peripheral blood. *Nat. Med.* **15**, 1088–1092 (2009).

doi:10.1038/nm.3358

European Journal of Immunology

Adipose tissue derived stromal stem cell therapy in murine ConA-derived hepatitis is dependent on myeloid-lineage and CD4$^+$ T-cell suppression

Mami Higashimoto[*1], *Yoshio Sakai*[*2,3], *Masayuki Takamura*[1], *Soichiro Usui*[1], *Alessandro Nasti*[1], *Keiko Yoshida*[1], *Akihiro Seki*[1], *Takuya Komura*[1], *Masao Honda*[3], *Takashi Wada*[2], *Kengo Furuichi*[4], *Takahiro Ochiya*[5] *and Shuichi Kaneko*[1,3]

[1] Disease Control and Homeostasis, Kanazawa University, Kanazawa, Japan
[2] Department of Laboratory Medicine, Kanazawa University, Kanazawa, Japan
[3] Department of Gastroenterology, Kanazawa University Hospital, Kanazawa, Japan
[4] Division of Blood Purification, Kanazawa University Hospital, Kanazawa, Japan
[5] Division of Molecular and Cellular Medicine, National Cancer Center Research Institute, Tokyo, Japan

Mesenchymal stromal stem cells (MSCs) are an attractive therapeutic model for regenerative medicine due to their pluripotency. MSCs are used as a treatment for several inflammatory diseases, including hepatitis. However, the detailed immunopathological impact of MSC treatment on liver disease, particularly for adipose tissue derived stromal stem cells (ADSCs), has not been described. Here, we investigated the immunomodulatory effect of ADSCs on hepatitis using an acute ConA C57BL/6 murine hepatitis model. i.v. administration of ADSCs simultaneously or 3 h post injection prevented and treated ConA-induced hepatitis. Immunohistochemical analysis revealed higher numbers of CD11b$^+$, Gr-1$^+$, and F4/80$^+$ cells in the liver of ConA-induced hepatitis mice was ameliorated after the administration of ADSCs. Hepatic expression of genes affected by ADSC administration indicated tissue regeneration-related biological processes, affecting myeloid-lineage immune-mediating Gr-1$^+$ and CD11b$^+$ cells. Pathway analysis of the genes expressed in ADSC-treated hepatic inflammatory cells revealed the possible involvement of T cells and macrophages. TNF-α and IFN-γ expression was downregulated in hepatic CD4$^+$ T cells isolated from hepatitis livers co-cultured with ADSCs. Thus, the immunosuppressive effect of ADSCs in a C57BL/6 murine ConA hepatitis model was dependent primarily on the suppression of myeloid-lineage cells and, in part, of CD4$^+$ T cells.

Keywords: Adipose tissue derived stromal stem cells · Anti-inflammatory effects · CD4$^+$ T cells · ConA hepatitis · Myeloid-lineage cells

Additional supporting information may be found in the online version of this article at the publisher's web-site

Correspondence: Dr. Shuichi Kaneko
e-mail: skaneko@m-kanazwa.jp

*These authors contributed equally to this work.

Introduction

Mesenchymal stromal stem cells (MSCs) are somatic cells that reside in the mesenchymal tissues, such as the BM, umbilical cord, and adipose tissue [1,2]. MSCs are able to differentiate into several types of cells (pluripotent) in the same lineage, such as chondrocytes, osteocytes, adipocytes, and cardiomyocytes, as well as those of different lineages, such as hepatocytes. Because of this differentiation capability, they have been studied as a possible application in regenerative therapy of miscellaneous impaired organs, such as breast reconstruction [3] and repair of ischemic heart tissue [4]. Another intriguing characteristic of MSCs is their immunomodulatory potency [5]. Because most liver diseases, including viral hepatitis [6,7], primary biliary cirrhosis [8], autoimmune hepatitis [9], and steatohepatitis [10], are associated with hepatic inflammatory cells [11], elucidation of the effect of MSCs on hepatic inflammation is important when considering the use of MSCs for treating liver diseases. Although the efficacy of MSC treatment of liver diseases has been reported [12], the detailed immunopathological impact of MSC treatment on liver diseases, particularly for adipose tissue derived stromal stem cells (ADSCs), has not been investigated.

ConA, a plant lectin [13], is frequently used to induce acute hepatitis in rodents [14] to model the pathological features of autoimmune hepatitis. Although this model is mediated mainly by lymphocyte-lineage cells such as T cells and NKT cells, Kupffer cells/macrophages also participate in hepatitis. Therefore, evaluating the therapeutic efficacy of ADSCs in this murine hepatitis model is important. Although the potential efficacy of ADSCs in a BALB/c ConA hepatitis model has been reported [15], the immunopathology has not been investigated.

We confirmed that immediate i.v. administration of ADSCs after ConA injection prevented hepatitis. We also observed that administering ADSCs 3 h after the ConA injection resulted in successful treatment of hepatitis, as the liver was already infiltrated by $CD11b^+$ and $Gr\text{-}1^+$ inflammatory cells. Gene expression analysis of the liver showed that ADSC treatment affected myeloid-lineage cells, providing repair and regenerative effects in ConA-induced hepatitis mice. Moreover, gene expression analysis of hepatic inflammatory cells indicated pathways related to T cells and monocyte-lineage cells. Pathologically important cytokines such as TNF-α and IFN-γ were upregulated in $CD4^+$ T cells isolated from ConA-induced hepatitis mice but were significantly suppressed by co-culture with ADSCs. Thus, the anti-inflammatory effects of ADSCs in the C57BL/6 murine ConA hepatitis model were mediated by the suppression of myeloid-lineage and $CD4^+$ T cells.

Results

Characteristics of the immune response in ConA-induced hepatitis mice

To examine the characteristics of ConA-induced acute hepatitis, we injected 300 μg ConA into C57BL/6 female mice ($n = 4$) and determined serum alanine transferase (ALT) and lactate dehydrogenase (LDH) activities. Serum ALT and LDH activities were elevated through 24 h (Fig. 1A). The macroscopic appearance and histology of the liver obtained 24 h after ConA injection revealed intense necrosis (Fig. 1B). The immunohistochemical analysis showed that the number of $CD4^+$ T cells in the liver peaked at 6 h after the ConA injection, and remained high for 24 h (Fig. 1C and D). The numbers of $CD11b^+$ cells and $Gr\text{-}1^+$ cells accumulated in the liver increased at 3 h and reached a maximum at 12 h after ConA injection (Fig. 1C and D). The numbers of $F4/80^+$ monocyte/macrophage lineage cells increased at 6 h after the ConA injection, but returned to basal levels after 24 h (Fig. 1C and D). We also assessed the frequency of $CD11b^+/Gr\text{-}1^+$ cells, as a phenotype of myeloid-derived suppressor cells (MDSCs), in ConA hepatitis mice at 6 h ($n = 3$). The frequency of $CD11b^+/Gr\text{-}1^+$ cells was higher than that in WT mice (Fig. 1E). Scavenger receptor CD204 expression was higher in $CD11b^+/Gr\text{-}1^+$ cells than $CD11b^+/Gr\text{-}1^-$ cells (Fig. 1F), and the population gated for $CD11b^+$ cells contained granulocytic $Ly\text{-}6C^+/Ly\text{-}6G^+$ cells as well as monocytic $Ly\text{-}6C^+/Ly\text{-}6G^-$ cells (Fig. 1G).

To determine the type of immune-mediating cells involved in ConA-induced acute hepatitis, we depleted mice of various immune cell subpopulations ($n = 4$ per group). Mice that were pretreated with clodronate, a reagent that depletes monocyte-macrophage lineage cells [16], followed by injection of ConA, did not show a significant elevation in serum ALT or LDH activity (Fig. 1H). Mild elevation of serum activity for these enzymes in mice depleted of $CD4^+$ T cells was observed, whereas depletion of $CD8^+$ T cells had no significant effect. These results suggest the importance of monocyte-macrophage myeloid-lineage cells, as well as the contribution of $CD4^+$ T cells, in ConA-induced hepatitis.

ConA-induced acute hepatitis is ameliorated by i.v. administration of ADSCs in vivo

Next, we determined the therapeutic efficacy of ADSCs in the ConA-induced hepatitis model. We obtained and expanded stromal cells from adipose tissue by passaging them eight to ten times (Fig. 2A). Almost all cells expressed the mesenchymal lineage markers, CD29 and CD44 (Fig. 2B). With regard to stem cell markers [17], approximately 40% and 73% of cells expressed CD105 and CD90, respectively (Fig. 2B). Moreover, the cells were pluripotent and were able to differentiate into osteocytes, chondrocytes, and adipocytes (Fig. 2C–F). When 1×10^5 ADSCs were administered via the tail vein immediately after ConA injection in mice ($n = 3$), the elevation of serum ALT and LDH activity was substantially ameliorated, compared with mice without ADSC treatment ($n = 4$) 24 h after injection (Fig. 3A). In terms of therapeutic efficacy, 1×10^5 ADSCs were administered to mice 3 h after ConA injection ($n = 3$), serum ALT and LDH activities were significantly reduced in acute hepatitis mice treated with ADSCs, compared with ConA-induced hepatitis mice without treatment ($n = 4$), 24 h after ConA administration (Fig. 3B). The macroscopic

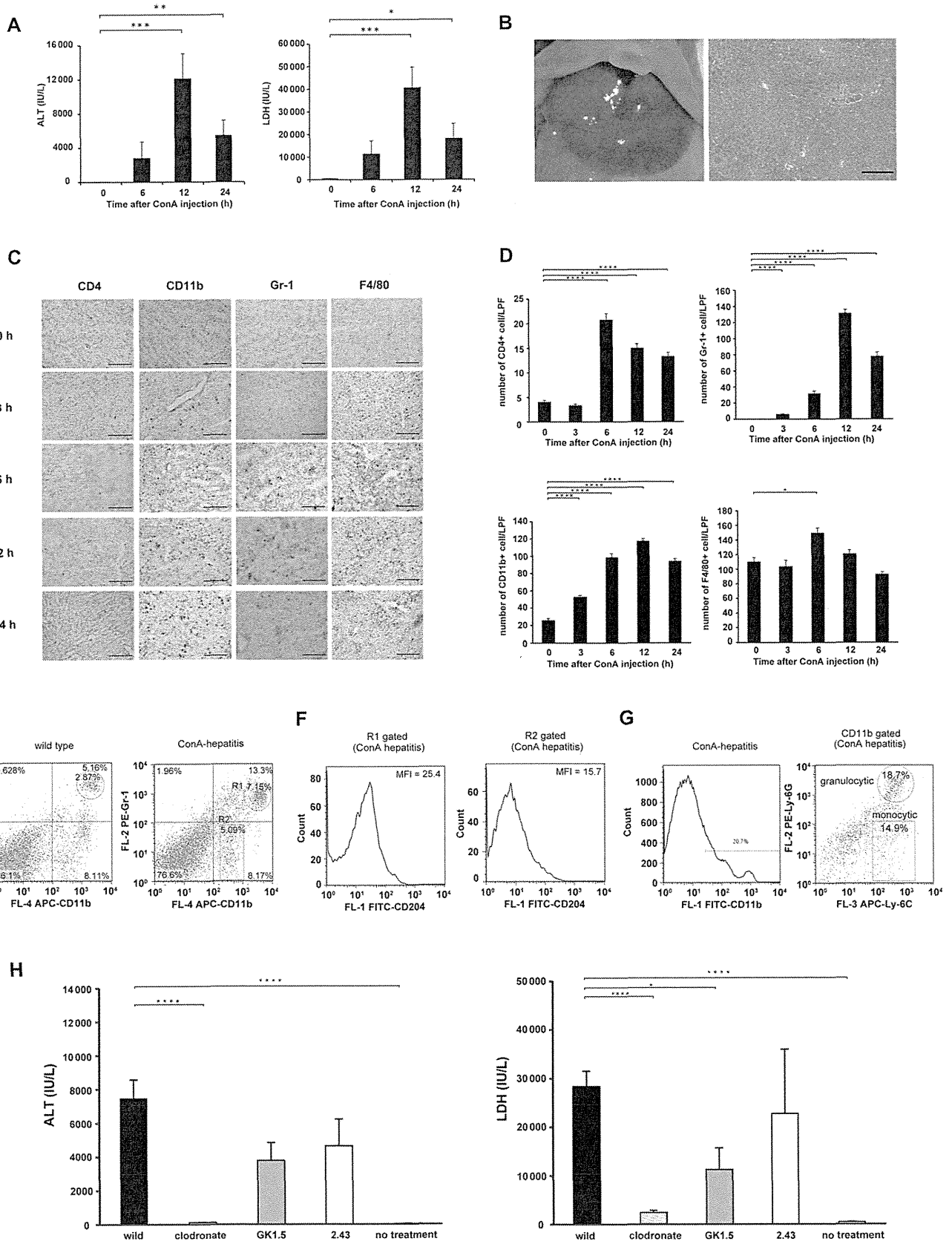

appearance of the liver obtained from mice injected with 300 μg of ConA followed by ADSC administration showed a mild and spotty white area with an almost normal color (Fig. 3C). Liver histology showed an almost normal appearance, with no necrosis (Fig. 3C), indicating that ConA-induced hepatitis was markedly ameliorated by ADSC treatment. No preventive or therapeutic effect on ConA-induced hepatitis resulted from administration of primary cultured murine hepatocytes ($n = 3$); there was no significant reduction in serum ALT or LDH (Fig. 3A and B), macroscopic necrosis appearance, or histological necrosis, compared with ConA-induced hepatitis (Fig. 3C).

ADSC treatment reduces elevated cytokine/chemokine concentrations in ConA-induced hepatitis mice

Marked protective and therapeutic effects of ADSCs on ConA-induced hepatitis were observed. To determine the effect of ADSC treatment on systemic inflammation in ConA-induced hepatitis, we measured serum cytokine and chemokine concentrations in ConA-induced hepatitis mice treated with ADSCs. Mice injected with ConA were immediately treated with ADSCs and serum was collected 6 h after ConA injection ($n = 3$). The elevated serum IFN-γ, IL-2, IL-6, IL-4, IP-10, MIG, KC, and MCP-1 levels in ConA-injected mice ($n = 3$) were significantly reduced by ADSC treatment (Supporting Information Fig. 1A). Injection of mice with ADSCs 3 h after ConA administration ($n = 4$) resulted in significantly reduced serum IFN-γ, IL-2, IL-6, and MIG levels, compared to ConA-injected mice not treated with ADSCs ($n = 6$) (Supporting Information Fig. 1B). Thus, the levels of the array of cytokines and chemokines that are elevated in the sera of ConA-induced hepatitis mice were significantly decreased by ADSC treatment.

Distribution of i.v. administered ADSCs in ConA-induced hepatitis murine models

The distribution of administered ADSCs in ConA-induced hepatitis mice was determined by immunohistochemistry. Administered GFP-expressing ADSCs were observed in the lung, but not the liver, of mice injected with ConA followed by immediate ADSC administration ($n = 6$), through 24 h (Supporting Information Fig. 2A). When administered to mice 3 h after ConA injection ($n = 6$), GFP-expressing ADSCs were observed primarily in the lung, and a few in the liver (Supporting Information Fig. 2B), suggesting that some fraction of ADSCs reached the liver upon occurrence of hepatitis.

Hepatic gene expression changes by ADSCs treatment are associated with Gr-1$^+$ and CD11b$^+$ cells

To investigate the detailed biological features of the liver in ConA-induced hepatitis mice that were treated with ADSCs, we examined the gene expression profiles of liver tissue of ConA-injected mice obtained 2 h after treatment with ADSCs using a DNA microarray. In the liver tissues of mice treated with ADSCs immediately after ConA injection ($n = 3$), 589 gene probes were differentially expressed compared with that in mice with ConA-induced hepatitis that had not been treated with ADSCs ($n = 3$). Expression of the majority of genes was downregulated by ADSCs, as shown by green color ($p < 0.05$; Fig. 4A). Principal component analysis using these genes showed a discernible distribution difference between the ADSC-treated and -untreated groups (Fig. 4B). When mice received ADSC treatment 3 h after ConA injection, hepatic expression of 309 gene probes was altered significantly compared with those in mice with ConA-induced hepatitis that had not been treated with ADSCs ($n = 3$). Expression of the majority of genes was downregulated by ADSCs, as shown by green color ($p < 0.01$; Fig. 4C). Principal component analysis of these genes also showed a discernible distribution difference between the ADSC-treated and untreated groups (Fig. 4D). In the context of biological maps of the genes affected by immediate ADSC treatment, cell differentiation, the inflammatory response, the DNA damage response, and apoptosis predominated (Supporting Information Table 1). In addition to these maps, tissue remodeling and wound repair, mitogenic signaling, and vascular development (angiogenesis) predominated in mice that had received ADSC treatment 3 h after ConA injection (Table 1), indicating that ADSCs provided not only anti-inflammatory effects, but also remodeling effects, in the ConA-damaged liver.

◀ **Figure 1.** Characteristics of ConA-induced hepatitis in C57BL/6 mice. (A–D) C57BL/6 female mice were injected i.v. with 300 μg of ConA. Sera and liver tissues were obtained 3, 6, 12, and 24 h after ConA injection. The data are representative of three individual experiments. (A) ALT and LDH activity in sera. Results are expressed as means ± SE ($n = 4$). $^*p < 0.05$, $^{**}p < 0.01$, $^{***}p < 0.005$ versus 0 h (Student's *t*-test). (B) Representative liver tissues obtained 12 h after ConA injection were assessed macroscopically and microscopically. Magnification: ×100. Bar: 200 μm. (C) Immunohistochemical staining for CD4, CD11b, Gr-1, and F4/80 in the livers of mice for each time point (0, 3, 6, 12, and 24 h; $n = 4$ per time point). Representative images of mice for each time point are shown. Magnification: ×100. Bar: 200 μm. (D) Quantification of the number of CD4$^+$, CD11b$^+$, Gr-1$^+$, and F4/80$^+$ cells in four visual fields per ×100 low-power field in the livers of representative mice in each group. Magnification: ×100. $^*p < 0.05$, $^{****}p < 0.001$ versus untreated mice (Student's *t*-test). (E–G) Hepatic inflammatory cells were isolated from mice 6 h after ConA injection, incubated with fluorescence-conjugated antibodies, and assessed by FACS. Three mice per group per experiment. Experiments were performed twice. (E) Frequency of CD11b$^+$Gr-1$^+$ cells in WT C57BL/6 mice and ConA hepatitis mice. (F) Analysis of CD204 expression in CD11b$^+$Gr-1$^+$ cells (R1-gated region in (E)) and CD11b$^+$Gr-1$^-$ cells (R2-gated region in (E)) among hepatic inflammatory cells from ConA hepatitis mice. MFI: mean fluorescence intensity. (G) CD11b$^+$ cells among hepatic inflammatory cells from ConA hepatitis mouse were gated, and Ly-6C and Ly-6G expression levels in the gated cells were determined. (H) C57BL/6 female mice were injected i.v. with clodronate ($n = 4$), i.p. with anti-CD4 antibody (GK1.5) ($n = 4$), or anti-CD8 antibody (2.43) ($n = 4$) every 24 h for 2 days. The mice were then injected i.v. with 300 μg of ConA. Sera were obtained 24 h after ConA injection, and ALT and LDH activities were then measured. Results are expressed as means +SE ($n = 4$ per group) and are representative of one experiment performed. $^*p < 0.05$, $^{****}p < 0.001$ versus ConA-injected WT mice ($n = 4$) (Student's *t*-test).

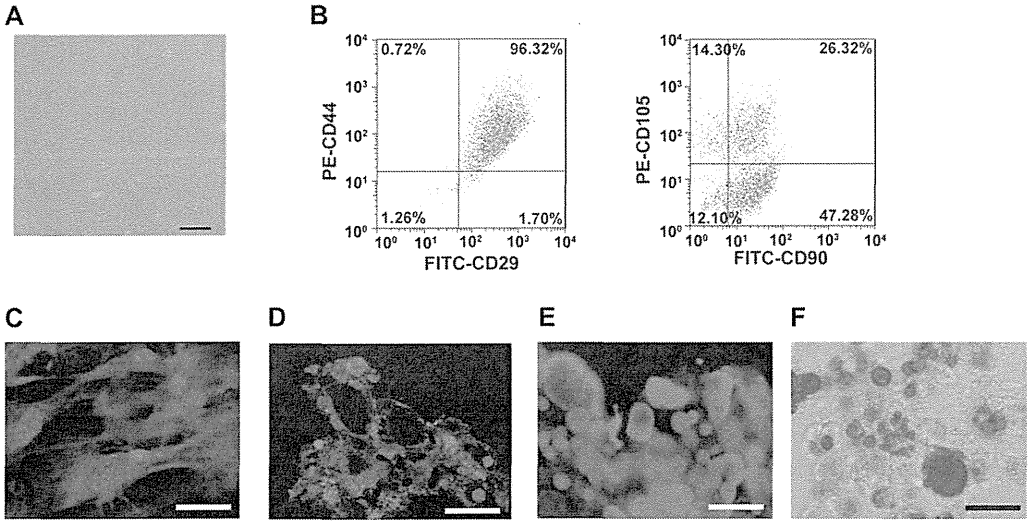

Figure 2. Characteristics and pluripotency of cultured ADSCs. Cells in the stromal fraction of adipose tissues from mice were cultured, maintained, and expanded for eight to ten passages. (A) Spindle shaped cells were observed after eight passages. Magnification: ×100. Bar: 200 μm. (B) Flow cytometric analysis of CD29, CD44, CD90, and CD105 surface marker expression. The data shown are representative of three independent experiments. (C–F) ADSCs were cultured with specific growth factors for induction of osteocytes, chondrocytes, and adipocytes using a mouse mesenchymal stem cell functional kit. Immunohistochemical staining was performed with (C) anti-osteopontin antibody for osteocytes, (D) anti-collagen II antibody for chondrocytes, and (E) anti-FABP antibody as well as (F) Oil-Red O staining for adipocytes. Magnification: x200. Bars: 50 μm. All data shown are from one experiment representative of two independent experiments performed.

Next, we investigated the relevance of these altered genes in the context of inflammatory cells using the public gene expression database of hematopoietic cells and stem cells (GSE27787). The annotated genes among the 589 gene probes detected by microarray analysis probes in the livers of mice that received ADSC treatment immediately after ConA injection were not relevant to any hematopoietic cell type (Fig. 4E). By contrast, among the 309 gene probes, the majority of the annotated genes whose hepatic expression in mice that received ADSC treatment 3 h after ConA injection was affected significantly were found to be highly expressed in Gr-1$^+$ cells and Mac1$^+$ (CD11b$^+$) cells — as indicated by the red color (Fig. 4F). Since majority of the 309 gene probes in the liver of ConA hepatitis were downregulated by ADSC treatment, as indicated by green color (Fig. 4C), these results suggested that effects on Gr-1$^+$ and CD11b$^+$ cells were associated with the therapeutic effect of ADSCs 3 h after ConA injection.

ADSC treatment represses inflammatory cell accumulation in ConA-induced hepatitis

To determine the influence of ADSC treatment on the infiltration/accumulation of immune-mediating cells in the liver of ConA-induced hepatitis mice, we assessed by immunohistochemistry the inflammatory cells in the liver tissues of mice injected with ConA followed by ADSC administration at 3 h. Liver tissues obtained at 6, 12, and 24 h ($n = 4$ each time point) after ConA injection showed reduced accumulation of CD11b$^+$ cells, Gr-1$^+$ cells, and F4/80$^+$ cells after ADSC treatment (Fig. 5). In contrast, the increased number of infiltrated CD4$^+$ T cells in ConA-induced hepatitis mice was not significantly affected by the ADSCs (Fig. 5). Thus, the predominant change in ConA-induced hepatitis mice treated with ADSCs was in the number of myeloid-lineage inflammatory cells, consistent with the hepatic gene expression data.

T-cell involvement in the altered gene expression of hepatic inflammatory cells by ADSCs treatment

To further assess the anti-inflammatory effects of ADSCs in mice with ConA-induced hepatitis, we isolated hepatic inflammatory cells from mice 2 h after ADSC treatment, which was administered 3 h after ConA injection ($n = 2$) and from mice not treated with ADSCs ($n = 2$). A total of 939 genes were differentially expressed in hepatic inflammatory cells from ConA-induced hepatitis mice treated with ADSCs. The gene expression profiles associated with ADSC treatment and ConA-induced hepatitis without ADSC treatment were readily distinguishable (Supporting Information Fig. 3A). Pathway map analysis showed that these genes were relevant to biological pathways of oncostatin M signaling via JAK-Stat or MAPK signaling and CCR5 signaling in macrophages and T lymphocytes in the immune response pathway (Supporting Information Table 2). Network analysis of these genes featured a network consisting of AcRIIA, STAT3, Activin A, FTSJD1, and STAT1 at the top (Supporting Information Table 3), which indicated that pathways involving IL-2 and TNF-α, and the STAT1/STAT3 pathway were also involved (Supporting Information Fig. 3B). These results suggest that T cells, as well as antigen presenting/phagocytosis lineages, were the immune-mediating cell populations affected by ADSC treatment.

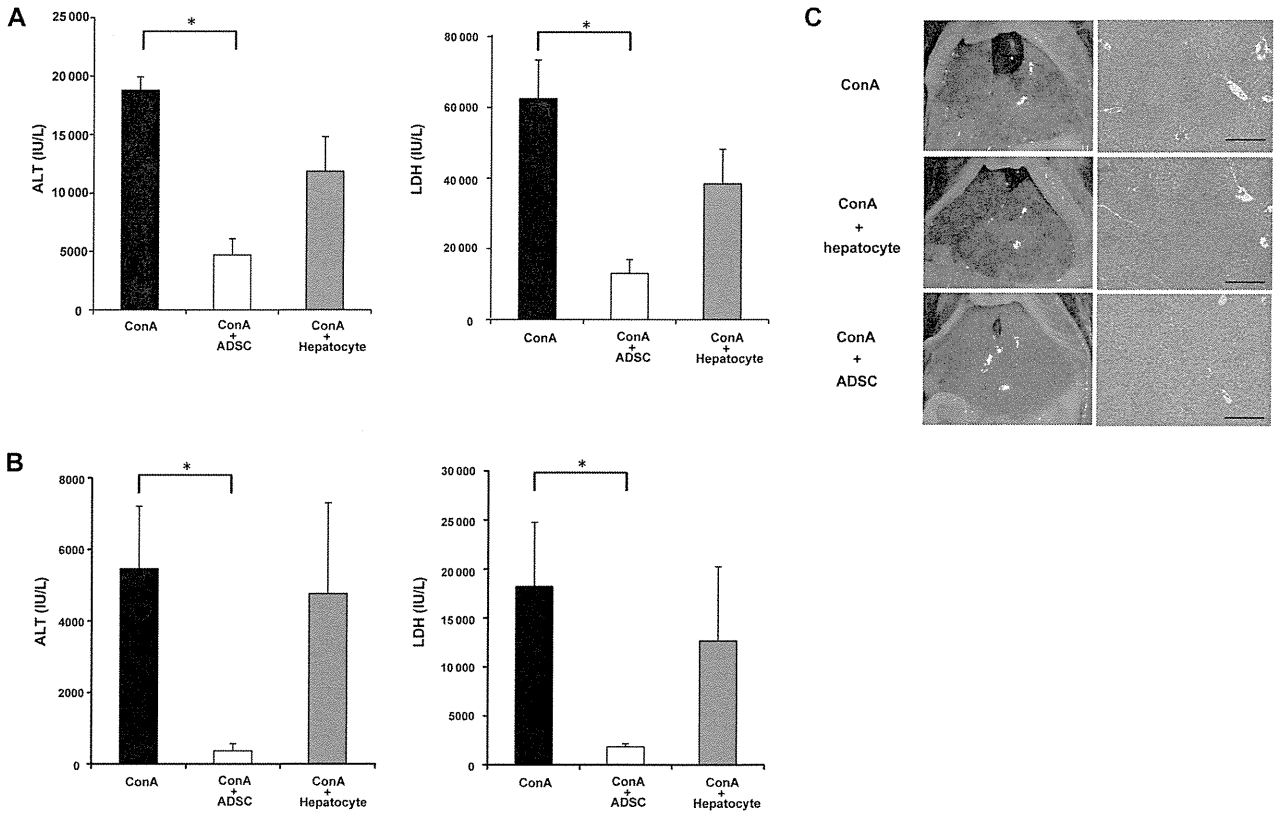

Figure 3. Therapeutic effects of ADSCs in ConA-induced hepatitis. C57BL/6 female mice were injected i.v. with 300 μg of ConA. Immediately or 3 h later, 1×10^5 ADSCs or hepatocytes were injected via the tail vein. Liver tissues and blood samples were obtained 24 h after ConA injection. Liver tissues were examined histologically and serum ALT and LDH activities were measured. (A, B) Serum ALT and LDH activities of mice injected with ConA followed by ADSC injection (A) immediately or (B) 3 h later. ConA: ConA-injected mice without treatment ($n = 4$), ConA + ADSC: ConA-injected mice followed by ADSC treatment ($n = 3$), ConA + hepatocyte: ConA-injected mice followed by primary cultured hepatocyte treatment ($n = 3$). Data are shown as mean ± SE and are from one experiment representative of two independent experiments. *$p < 0.05$ (Wilcoxon signed-rank test), compared with ConA-injected mice. (C) Macroscopic appearance of the liver (left) and histology of the liver tissues as assessed by H&E staining (right). Magnification of histology: ×100. Bars: 200 μm. Images shown are from one mouse representative of three to four mice from each group studied.

ConA-activated CD4$^+$T cells and CD11b$^+$ cells in the liver are important targets of ADSC treatment

The above data indicated that ADSCs administered in ConA-induced hepatitis had therapeutic immunological effects in terms of repairing the damaged liver and affected CD11b$^+$ and Gr-1$^+$ myeloid-lineage cells and T cells. To further explore how ADSCs affected the subpopulations of inflammatory cells involved in ConA-induced hepatitis, we investigated the expression of cytokine/chemokine-related genes in CD4$^+$ T cells and CD11b$^+$ cells obtained from livers with ConA-induced hepatitis ($n = 4$) that had been treated in vitro with ADSCs ($n = 3$). Expression of TNF-α, IL-10, and CXCL10 was significantly downregulated by ADSC treatment in both CD4$^+$ T cells (Supporting Information Fig. 4A) and CD11b$^+$ cells (Supporting Information Fig. 4B). IFN-γ, IL-4, and CXCL9 expression by CD4$^+$ T cells were significantly affected by ADSCs. Although CCL3, which was upregulated by ConA injection, was not significantly affected by ADSCs, the expression of its cognate receptor, CCR5, was decreased in CD4$^+$ T cells (Supporting Information Fig. 4A), suggesting an effect on the CCL3-CCR5 axis. These results suggest that CD4$^+$ T cells and myeloid-lineage CD11b$^+$ cells were the susceptible hepatic inflammatory subpopulations of cells in the ConA-induced hepatitis liver.

Anti-inflammatory effect of ADSCs on ConA hepatitis do not rely on MDSCs

We further assessed whether the anti-inflammatory effect of ADSCs in ConA hepatitis relied on MDSCs. Neither the frequency of nor the NO production by CD11b$^+$Gr-1$^+$ cells were increased by ADSC treatment (Supporting Information Fig. 5A). CD11b$^+$Gr-1$^+$ cells from ConA-injected mice treated with ADSCs showed arginase activity similar to that in CD11b$^+$Gr-1$^+$ cells from ConA-injected mice (Supporting Information Fig. 5B). CD11b$^+$Gr-1$^+$ cells from ConA-injected mice treated with ADSCs suppressed the ConA-stimulated proliferation of T cells in vitro, although the effect was slightly attenuated compared to that of cells from mice with ConA-induced hepatitis (Supporting Information Fig. 5C). Thus, ADSC treatment was not dependent on MDSCs induced by ConA hepatitis.

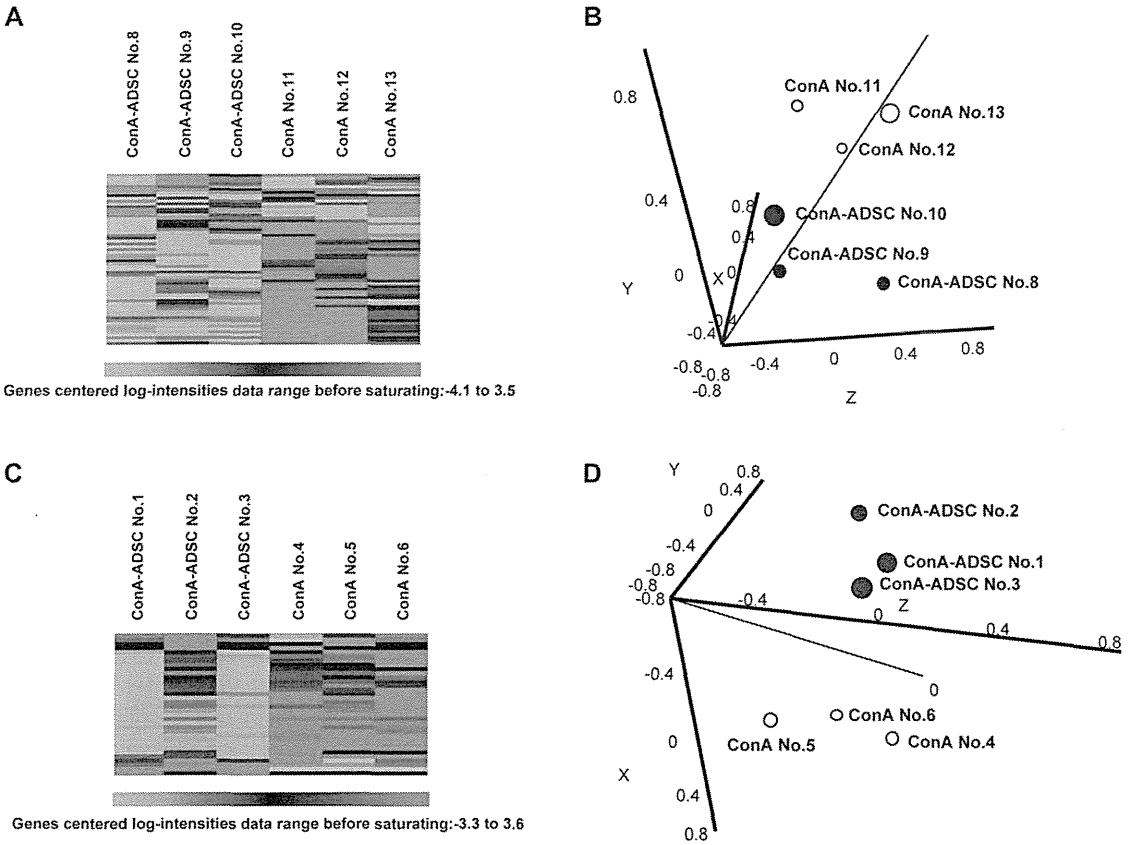

Discussion

MSCs are effective for immune-mediated disease treatment including the ConA-induced BALB/c murine hepatitis model [15], but the detailed mechanisms have not been fully elucidated. Here, we confirmed that ADSCs have preventive and therapeutic effects in a ConA-induced C57BL/6 hepatitis murine model and assessed the immunopathological mechanisms by determining the participating hepatic immunomodulatory cells. ADSCs injected via the tail vein were found in the lung; some were observed in the liver but only when ADSCs were administered 3 h after ConA injection, a time at which infiltration of $CD11b^+$ and $Gr\text{-}1^+$ inflammatory cells into the liver had already begun. Gene expression analysis of liver tissue from ConA-induced hepatitis mice showed that the ADSC treatment induced biological pathways indicative of liver repair and regeneration. Myeloid-lineage cells were the predominant population in terms of affected genes, consistent with immunohistochemical staining of the liver for immune-mediating cells. Furthermore, the gene expression profiles of hepatic inflammatory cells from ConA-induced hepatitis mice treated with ADSCs suggested T-cell and macrophage involvement. Moreover, the expression patterns of cytokine/chemokine-related genes in hepatic inflammatory cells co-cultured with ADSCs suggested that $CD4^+$ T cells were important in ConA-induced hepatitis and were affected by ADSC treatment.

The immunopathological features of ConA-induced hepatitis have been characterized as being primarily lymphocyte-lineage cell-mediated hepatitis [18–20], leading to massive hepatocellular degeneration, necrosis, and apoptosis [21]; thus, this model is relevant to clinical autoimmune hepatitis. Additionally, Kupffer cells play an important role in induction of hepatitis [22]. Unexpectedly, we observed prominent increases in $CD11b^+$, $Gr\text{-}1^+$, and $F4/80^+$ cells in liver tissues of the ConA-induced hepatitis mice. Additionally, we found that the monocyte-macrophage lineage cells contributed most significantly to hepatitis, as confirmed by depletion treatment, such that hepatitis was almost completely abolished when those cell types were abrogated by clodronate. This is further evidenced by the fact that ADSC treatment reduced the number of $CD11b^+$, $Gr\text{-}1^+$, and $F4/80^+$ cells in the liver of ConA-induced hepatitis mice (Fig. 5). The importance of $Gr\text{-}1^+$ and $CD11b^+$ cells was also suggested by changes in the gene expression profile of the liver of ConA-induced hepatitis treated with ADSCs (Fig. 4C and F). Thus, monocyte-macrophage lineage cells are important in the pathogenesis of ConA-induced hepatitis in mice and are important targets of ADSCs. $CD4^+$ T cells were also involved since their depletion partially ameliorated ConA-induced hepatitis. The number of infiltrating $CD4^+$ T cells in the liver of ConA-induced hepatitis mice was not markedly reduced by ADSC treatment. However, gene expression analysis of hepatic inflammatory cells in ConA-induced hepatitis mice treated with ADSCs showed that signaling of oncostatin M, a type I cytokine associated with developing T cells [23], and CCR5 signaling in macrophages and T lymphocytes were affected. Therefore, $CD4^+$ T cells participate as an immune mediator and therapeutic target of ADSCs in the pathology of ConA-induced hepatitis mice.

With regard to cytokine/chemokine-related gene expression in hepatic inflammatory cells of ConA-induced hepatitis mice, expression of TNF-α, IL-10, and CXCL10 in $CD4^+$ T cells and $CD11b^+$ cells was downregulated by ADSC treatment (Supporting Information Fig. 4). Additionally, IFN-γ, IL-4, and CXCL9 were also significantly downregulated in $CD4^+$ T cells, but not in $CD11b^+$ cells (Supporting Information Fig. 4). Changes in the expression of the Th2 cytokines, IL-10 and IL-4, were considered to be the secondary consequence of ConA-induced hepatitis, mediated by TNF-α and/or IFN-γ, which are characterized as Th1-associated cytokines [24]. CCR5 expression by $CD4^+$ T cells was downregulated by ADSCs, which may be relevant to the biological processes indicated by the downregulated genes in hepatic inflammatory cells. Because CCR5 is a $CD4^+$ T-cell receptor that interacts with APCs, such as macrophages [25], suppression of CCR5 expression on $CD4^+$ T cells by ADSC might explain the amelioration of ConA-mediated hepatitis. Overall, the therapeutic efficacy of ADSCs impacted both $CD4^+$ and $CD11b^+$ cells in terms of alteration of levels of inflammatory humoral mediators and cytokine/chemokine profiles, thus contributing to amelioration of ConA-induced hepatitis.

A proportion of i.v. administered ADSCs were present in the livers of ConA mice injected with ADSCs at a time point at which the liver had already been infiltrated with $Gr\text{-}1^+$ and $CD11b^+$ cells, whereas no ADSCs were present in the livers of mice injected with ConA following immediate treatment with ADSCs. This indicates that a liver undergoing inflammation attracts administered ADSCs. The extent of inflammation required to recruit ADSCs should be clarified, as it has previously been reported that hepatitis occurring just 30 min after ConA injection results in recruitment of a substantial number of stem cells to the liver in the BALB/c ConA hepatitis model [15]. Given that the migratory capabilities of MSCs are well known although not yet fully investigated [26], how ADSCs are recruited to an already inflamed liver as a result of ConA administration should be examined. In addition, the ADSCs administered to C57BL/6 mice immediately after ConA injection resided in the lung. In spite of the fact that they were not detected in the liver, these ADSCs prevented ConA hepatitis, indicating the remote effect of ADSCs. Thus, indirect mediators produced by ADSCs associated with their anti-inflammatory effects should be investigated intensively.

◀ **Figure 4.** Gene expression analysis in the liver of ConA-induced hepatitis mice treated with ADSCs. C57BL/6 female mice were injected i.v. with 300 μg of ConA. (A, B, and E) Immediately or (C, D, and F) 3 h after ConA injection, mice were treated with 1×10^5 ADSCs via the tail vein ($n = 3$ each). Liver tissues were analyzed 2 h after ADSC administration and RNA was isolated for gene expression analysis using a DNA microarray. Data shown are from one experiment performed. (A, B) One-way clustering analysis (A) and principal component analysis (B) of the 589 differentially expressed genes in treated and untreated ConA-injected mice. (C, D) One-way clustering analysis (C) and principal component analysis (D) of the 309 differentially expressed genes in treated (after 3 h) and untreated ConA-injected mice followed. Colors indicate the intensity of gene upregulation (red), downregulation (green), and no change (black). (E, F) One-way clustering analysis of gene expression in hematopoietic and stem cells (GSE27787) for annotated genes among the 589 (E) and 309 (F) genes.

Table 1. Maps relevant to genes for which the expression was affected in the liver of ConA-injected mice followed by ADSC treatment at 3 h.

Maps	*p*-value
Tissue remodeling and wound repair	0.000001438
Inflammatory response	0.000003973
Mitogenic signaling	0.0001056
Vascular development (angiogenesis)	0.0002926
DNA damage response	0.0004529
Apoptosis	0.0008909
Cystic fibrosis disease	0.001402
Myogenesis regulation	0.001571
Cell differentiation	0.002173
Immune system response	0.003304

In conclusion, the therapeutic anti-inflammatory efficacy of ADSCs relied on suppression of myeloid-lineage and $CD4^+$ T cells in the ConA-induced C57BL/6 murine hepatitis model. The application of ADSC therapy to various inflammatory liver diseases can be further developed by studies of their immunomodulatory effects.

Materials and methods

Murine acute hepatitis induced by ConA injection and treatment with ADSCs

C57BL/6J female mice (10–12 weeks old, Charles River Laboratories Japan Inc., Yokohama, Japan) were injected i.v. with 300 μg of ConA (Sigma-Aldrich, St. Louis, MO, USA) dissolved in PBS. For $CD4^+$ T-cell or $CD8^+$ T-cell depletion, 200 μg of purified anti-CD4 antibody from the culture supernatant of GK1.5 cells (ATCC, Manassas, VA, USA), or purified anti-CD8 antibody from the culture supernatant of 2.43 cells (ATCC), was injected i.p. for two consecutive days before ConA injection. For depletion of monocyte-macrophage lineage cells, 2 mg of clodronate (Sigma-Aldrich), which was encapsulated in liposomes using the COATSOME-EL-01-N liposome formulation kit (Nihonyushi, Tokyo, Japan) [27], was injected via the tail vein 2 days before ConA injection. For the prevention or treatment experiment, 1×10^5 ADSCs were administered i.v. immediately or 3 h after ConA injection. In some cohorts, blood was obtained under anesthesia, and liver and lung tissues were collected after euthanizing mice at 6, 12, and 24 h after ConA injection. A portion of the liver tissue was homogenized and the enriched fraction of inflammatory cells was obtained by gradient centrifugation using Ficoll–Hypaque (Sigma-Aldrich). Our institutional review board approved the care and use of laboratory animals in all experiments.

Isolation and culture of ADSCs and primary hepatocytes

Inguinal adipose tissues were obtained from C57BL/6J male mice (10–12 weeks old, Charles River Laboratories Japan Inc.) or GFP-transgenic mice (male, 10–12 weeks old, gift from Prof. Okabe, Osaka University, Japan). Tissues were digested with 0.075% collagenase type I (Wako Pure Chemical Industries Ltd., Osaka, Japan), washed with PBS, and then transferred to a culture dish with DMEM/F-12 1:1 medium (Life Technologies–Invitrogen, Carlsbad, CA, USA) supplemented with 10% heat-inactivated FBS and 1% antibiotic–antimycotic solution (Life Technologies). Cells were maintained and expanded by eight to ten passages before use.

To obtain primary hepatocytes, C57BL/6J male mice (10–12 weeks old) were anesthetized by i.p. injection of pentobarbital (50 mg/kg; Kyoritsu Seiyaku, Tokyo, Japan) and injected with 10 mL of 0.75% type I collagenase solution via the portal vein. Liver tissues were minced to dissociate cells, filtered through a 100 μm mesh, and cultured in 10-cm culture dishes for 16 h until use.

Pluripotency of ADSCs

The pluripotency of ADSCs was examined using a mouse mesenchymal stem cell functional kit® (R&D Systems, Minneapolis, MN, USA), and immunohistochemical staining of cells that had differentiated into osteocytes, chondrocytes, and adipocytes was performed using anti-mouse ostepontin, anti-mouse collagen II, and anti-mouse FABP4 antibodies, respectively, in accordance with the manufacturer's instruction. Adipocyte differentiation was also assessed by staining using an aliquot of Oil Red O (WAKO).

Co-culture of ConA-stimulated hepatic inflammatory cells with ADSCs

Hepatic inflammatory cells were isolated from C57BL/6J female mice (10 weeks old) that had been injected i.v. with 300 μg of ConA 3 h before ($n = 4$). $CD4^+$ T cells and $CD11b^+$ cells were separated from the collected hepatic inflammatory cells using anti-CD4 and anti-CD11b magnetic beads (Miltenyi Biotec, Bergisch Gladbach, Germany). Then, 20 000 ADSCs were co-cultured with 4×10^5 of the isolated $CD4^+$ T cells or $CD11b^+$ cells in a 24-well plate (BD Falcon, San Jose, CA, USA) for 2 h ($n = 3$). After co-culture, floating cells were harvested, and RNA harvested using the MicroRNA isolation kit (Stratagene, La Jolla, CA, USA) for real-time PCR analysis to measure cytokine/chemokine gene expression.

Measurement of serum ALT and LDH activity

Blood was collected from the postorbital venous plexus and serum was separated from clotted blood after coagulation. The serum activity of ALT, and LDH was measured using L-type WAKO GPT J2, and LDH-J kits (Wako Pure Chemical Industries Ltd.), respectively, using autoanalytical equipment (Hitach7180, Hitachi Ltd., Tokyo, Japan), according to the manufacturer's protocol.